In search for a gold-standard procedure to count motor neurons in the spinal cord

Michela Ferrucci[1], Gloria Lazzeri[1], Marina Flaibani[1], Francesca Biagioni[2], Federica Cantini[1], Michele Madonna[2], Domenico Bucci[2], Fiona Limanaqi[1], Paola Soldani[1], Francesco Fornai[1,2]

[1]Department of Translational Research and New Technologies in Medicine and Surgery, Human Anatomy, University of Pisa, Pisa, Italy.

[2]Istituto di Ricovero e Cura a Carattere Scientifico, Neuromed, Pozzilli, Isernia, Italy.

Correspondence
Francesco Fornai
Human Anatomy, Dept of Translational Research and New Technologies in Medicine and Surgery
University of Pisa
Via Roma 55 – 56126 Pisa (Italy)
Tel: +39 050 2218611
email: francesco.fornai@med.unipi.it

Running title: stereology-like count of motor neurons

Keywords: stereology, spinal cord, brainstem, motor neurons, light microscopy.

Summary

Counting motor neurons within the spinal cord and brainstem represents a seminal step to comprehend the anatomy and physiology of the final common pathway sourcing from the CNS. Motor neuron loss allows to assess the severity of motor neuron disorders while providing a tool to assess disease modifying effects. Counting motor neurons at first implies gold standard identification methods. In fact, motor neurons may occur within mixed nuclei housing a considerable amount of neurons other than motor neurons. In the present review, we analyse various approaches to count motor neurons emphasizing both the benefits and bias of each protocol. A special emphasis is placed on discussing automated stereology. When automated stereology does not take into account site-specificity and does not distinguish between heterogeneous neuronal populations, it may confound data making such a procedure a sort of "guide for the perplex". Thus, if on the one hand automated stereology improves our ability to quantify neuronal populations, it may also hide false positives/negatives in neuronal counts. For instance, classic staining for antigens such as SMI-32, SMN and ChAT, which are routinely considered to be specific for motor neurons, may also occur in other neuronal types of the spinal cord. Even site specificity within Lamina IX may be misleading due to neuronal populations having a size and shape typical of motor neurons. This is the case of spinal border cells, which often surpass the border of Lamina VII and intermingle with motor neurons of Lamina IX. The present article discusses the need to join automated stereology with a dedicated knowledge of each specific neuroanatomical setting.

1. Introduction

Being investigators in neuroanatomy, we are all familiar with reviewers' criticisms involving the lack of an automatic stereology software when assessing neuronal loss or neuronal integrity. While an accurate stereological procedure may increase the reliability of quantitative data, at the same time this may be misleading when routinely applied within a heterogeneous group of neurons. A rigid automated count of motor neurons (MNs) carried out without a firm grasp of the fine anatomical specificities of a given motor nucleus may provide just a "scientific halo" covering the crude complexity of biological facts and cutting corners in describing anatomical facts which are rather more complex. The present article is an attempt to join the advantages of automated stereology with the need for flexibility coming from dedicated neuroanatomical observations. Thus, a detailed knowledge of the fine neuroanatomy of specific motor nuclei needs to be preliminarily considered before choosing the best procedure to obtain reliable counts of MNs. The co-existence of MNs with neurons other than MNs within the same nucleus, which is grossly classified as a "motor nucleus", does occur quite often making it mandatory to possess an in depth knowledge of a given motor nucleus before quantifying its cells as MNs as a whole.

Such an in depth knowledge is often acquired by a plain literature search, though an empirical pilot characterization of authentic MNs is needed in each specific experimental setting, as a preliminary step before quantifying cells within a motor nucleus. This is required in baseline (control) conditions and becomes a key point during a traumatic or degenerative disorder. In fact, in these latter conditions a shift in neuronal phenotype may confound those size and shape criteria, which are routinely used as a reference to identify motor cells (i.e. the enlargement of MN soma, which occurs in amyotrophic lateral sclerosis, ALS), thus altering the size exclusion criteria in MN counts. Similarly, disease-dependent phenotypic shifts may affect specific antigens, such as SMI-32 and SMN (i.e. survival MN protein), which need always to be considered before prompting MN counts.

2. Historical overview of motor neuron identification

From an historical perspective, dating back to the introduction of immunohistochemistry, MNs were characterized based on their shape. By using this approach, a detailed description of MNs in the human spinal cord was provided in 1854 by the Swiss anatomist Rudolf Albert Von Kölliker, who defined these "motor cells" as "[…] very remarkable in their size, […], being 67 to 135 μm in diameter, a nucleus of 11 to 18 μm […] fusiform or polyhedral, […]; 2 to 9 large processes, sometimes more, […], depart from their end" (Von Kölliker, 1854). By using Golgi's reaction, Von Kölliker identified the site-specificity of these "motor cells". In detail, he indicated the occurrence of large motor cells within the ventral aspect of the anterior horn of the spinal cord, whereas smaller motor cells were described in the medial part of the anterior horn and dorsally, between the anterior and posterior horns (Von Kölliker and Turner, 1891). Nonetheless, this pioneer description shows discrepancies among MN populations concerning site- and size-variability, which still continues to be a critical point when counting MNs nowadays. When observed following Golgi staining MNs were originally defined as those neurons generating an axon coursing out from the grey matter to join the anterior roots, through straight or arched directions. Von Kölliker (Von Kölliker and Turner, 1891) noticed the presence of axon collaterals but he did not focus his analysis on this cell process. This was previously described by Santiago Ramón y Cajal (1889), who indicated an axonal branch coursing backwards (later identified as the recurrent collateral of MNs). When Von Kölliker early described MNs, he still considered these cells as distinct from classic neurons within the central nervous system (CNS). In fact, Von Kölliker emphasized the role of what he named "nerve cells" as the source of the ventral root but keeping them distinct from neurons described within the CNS, which send their axons to areas within the CNS itself. Such an historical perspective was detailed in the exhaustive review by Clarac and Barbara (2011). The concept of nerve cells, as it was developed by Von Kölliker, was conserved by other eminent anatomists such as Deiters, Golgi, Von Gerlach, and Clarke, who from different perspectives, considered these cells as unique, differing from classic neurons (Clarac and Barbara, 2011). Santiago Ramón y Cajal firmly rejected

this concept and he considered nerve cells as equivalent to classic neurons (Ramón y Cajal, 1911). In fact, the term "motor neurons" (literally "célula nerviosa motora") was used first by Ramón y Cajal to emphasize the similarity between such neurons forming peripheral nerves and those CNS neurons connecting areas posed at short and long distances but remaining confined within the same CNS.

A comprehensive definition of what we now consider as MN was further provided by Ramón y Cajal, in the context of the "neuron theory", when he first used the term "motor neurons" referring to distinct nervous cells, lying within the ventral horn of the spinal cord and sending branches through the ventral roots to reach skeletal muscles (Ramón y Cajal, 1911). In his seminal work, Ramón y Cajal emphasized specific anatomical criteria (site, size, shape and axonal fate) in order to classify a neuron as authentic "motor neuron" ("célula nerviosa motora"). These anatomical criteria remained steady along decades and are still key in practical stereology. Ramón y Cajal provided very many details about MN's cell body, axon, and dendrites simply based on light microscopy carried out on samples stained through his modified Golgi's method. As usual for his studies, he provided talented descriptions and predictions without the aid of electron microscopy, although these descriptions were fully confirmed by later electron microscopy observations.

A number of studies carried out by a British team of neuropathologists compared different methodological procedures to count MNs within the lumbo-sacral segments of the human spinal cord. These authors described step by step the experimental protocol, including detailed information about tissue preparation, sections cut and collection, and they provided histological criteria for identifying MNs (Tomlinson et al.; 1973; Irving et al., 1974; Tomlinson and Irving, 1977). In these papers, the identification of MNs was based on morphometry and topography. As a paradox, MNs became the paradigm to describe the anatomy and physiology of the neuron. In fact, the large MN size along with its superficial placement within the spinal cord and the chance to easily identify and isolate its long axon all represent ideal features for anatomists and electrophysiologists.

All over the present review, the terms “anterior horn” and “posterior horn” are used in humans and refer to the homologous aspects of the spinal cord grey matter of rodents, which are referred indeed as “ventral horn” and “dorsal horn”, respectively.

3. How motor neurons are currently identified

The first feature which identifies MNs is their specific topography. Somatic MNs are large multipolar neurons lying within the ventral horn of the spinal cord and the motor nuclei of the brainstem, divided into alpha- and gamma-MNs, based on their innervation of extrafusal or intrafusal muscle fibers, respectively. In the spinal cord, alpha- and gamma-MNs are intermingled within the ventral horn, at the level of the Lamina IX of the grey matter (Rexed, 1952). In addition to somatic MNs, autonomic MNs (or beta-MNs) are placed within the dorso-lateral extent of the ventral horn, within Rexed’s Lamina VII. When it is not specified otherwise, in the present review we refer to somatic alpha-MNs (from here on simply indicated as MNs), as they are specifically affected in MN disorders.

In particular, MNs lie in the anterior part of the anterior horn; when they are abundant, they organize into three major columns: an anteromedial column, which extends continuously throughout the whole spinal cord, and an intermediate and an anterolateral column, which occur only at the cervical and lumbosacral enlargements. This peculiar topography of MNs reflects a specific somatotopy of the peripheral muscles they supply: MNs in the anteromedial column innervate axial muscles, MNs in the intermediate column innervate proximal muscles of the limbs and those in the anterolateral column innervate distal muscles of the limbs.

The second feature identifying MNs is the size of their soma. MNs are generally described as the largest neurons of the anterior/ventral horn, although their size might vary in different animal species and even strains, and along different segments of the spinal cord (Elliott, 1942, 1944; Romanes, 1951; Fulceri et al., 2012). In particular, the type of innervated muscle fibers (“slow” for “tonic” and “fast” for “phasic” motor units), and their relative size (generally smaller in “tonic” and

wider in “phasic” motor units), represent the major determinants of MN size: large MNs generally supply phasic muscle fibers, while small MNs generally innervate tonic muscle fibers. In humans, the size of MN cell body ranges between 30 μm up to over 100 μm, with the largest MNs being confined to the anterolateral column (Truex and Carpenter, 1969; Tomlinson et al., 1973; Oda et al., 1995; McBride and Schmorrow, 2005). In other mammals, MNs’ cell bodies are generally smaller in size, measuring on average 30-35 μm in rodents (Martin et al., 2007; Fornai et al., 2008a) and 55 μm in cats (Brown and Fyffe, 1981), according to the smaller size of the muscle fibers they supply.

The third feature identifying MNs is their shape under histochemical observation. When using cresyl violet or haematoxylin & eosin (H&E) staining, MNs appear as basophilic multipolar cells owning a large and pale nucleus with scarcely condensed chromatin (euchromatin), intensely labelled nucleoli, and basophilic material filling the cytosol, consisting of a high amount of ribosomal-enriched organelles (i.e. granular endoplasmic reticulum, aggregated polyribosomes) and aggregates of mRNA molecules within aggreosomes (Figure 1). These basophilic organelles were originally indicated as “Nissl substance” or “Nissl bodies”, or “tigroid bodies”, referring to the peculiar “striped” feature of the MN cytosol (Huisinga et al., 2006; Thompson, 2000). The term “chromatolysis” indicates the decrease of cytosolic basophilic bodies, which occurs in degenerating MNs due to disaggregation of Nissl bodies (Goldstein et al., 1987). Remarkably, retrograde chromatolysis, induced by peripheral nerve section or ventral root avulsion, represented a common procedure to identify MNs (Romanes, 1964).

All these morphological features described as they appear at light microscopy are characterized in detail at ultrastructural level, where MNs show a large, round-shaped nucleus, with a prominent nucleolus, and a wide, electron-dense cytosol, with abundant neurofilaments, GERL (acronym for Golgi apparatus, endoplasmic reticulum and lysosomes)-related structures and mitochondria. Light microscopy analysis of MNs, detailing placement, size, shape and histochemistry does not positively discriminate MNs from neighboring neurons. For instance, Renshaw cells, which receive

recurrent collaterals from MNs and in turn inhibit MNs, lie very close to MNs, within the ventral extent of Lamina VII. Despite the small size and different morphology of Renshaw cells compared with MNs, in pioneer studies their proximity to MNs led to their misidentification (Ramón y Cajal, 1909; Eccles et al., 1954; Romanes, 1964). Other neurons, which lie close by and histochemically overlap with MNs are the spinal border cells (SBCs, Cooper and Sherrington, 1940). Spinal border cells represent the origin of the ventral and rostral spinocerebellar tract, with their axons crossing the midline to reach the cerebellum. These large neurons, lying preponderantly "in the fringe of the grey matter bordering the ventrolateral grey matter" (Cooper and Sherrington, 1940) may be distinguished in two pools, one lying near the dorsolateral border of the ventral horn and the other scattered within the lateral and medial portion of the ventral horn (Sprague, 1953; Hubbard and Oscarsson, 1961; Burke et al., 1971). In spinal cord preparations stained with the Golgi's method SBCs were reported to differ from MNs due to shorter dendritic trees and Nissl bodies' arrangements (Ha and Liu, 1968; Romanes, 1964).

Axon tracking is a classic MN identification method based on the fact that MNs' axons eventually innervate peripheral muscles. Therefore, an intramuscular injection of a dye, which is retrogradely transported to the perikaryon without passing the synaptic cleft, is expected to selectively stain MNs (or at most, in combination with neurons innervated by MN axon collaterals). This technique takes advantage of the ability of nerve axons to take up specific dyes and transport them retrogradely, thus providing information about the place of single MNs within the CNS and their peripheral connections. For instance, retrograde labelling of MNs by injecting horseradish peroxidase (HRP) into a given muscle represents a common procedure to track which MN innervates such a muscle (Kristensson and Olson, 1971; LaVail and LaVail, 1972; Oppenheim and Heaton, 1975; Mesulam, 1978; Sohal and Holt, 1978; Hopkins and Armour, 1998; Harding et al., 1999; White et al., 2000; Ramanathan et al., 2006). The mechanisms underlying this technique consist of: i) the uptake of HRP via endocytosis/pinocytosis; ii) retrograde axon transport through micro-tubules, using dynein as the driver molecule; iii) an enzymatic reaction between H_2O_2 and an exogenous chromogen

catalyzed by HRP; iv) a stained reaction product that precipitates within the neuron, making it visible at light microscopy. In recent years, neuroanatomical tracking was improved by enriching the tracking techniques, throughout ionto-phoretic application of the tracer or by applying crystal dye which enters directly into transected axonal fibers. In MN studies, improvements were mostly achieved by using tracers other than HRP, such as fluorescent probes (Richmnond et al., 1994; Sauer and Oertel, 1994; Haenggeli and Kato 2002a; Barazzoni et al., 2005; Dudek et al., 2011; Karalija et al., 2012; Skup et al., 2012; Fu et al., 2014), labeled muscle toxins (Buttry and Goshgarian, 2015; Jara et al., 2014; Mantilla et al., 2009) and retrograde virus-mediated trans-synaptic tracers (i.e. rabies virus) (Rice et al., 2010; Ugolini, 2011; Ishida et al., 2015; Kasumacic et al., 2015; Li et al., 2015; Xu et al., 2015). However, the technique is invasive and specificity/sensitivity may be reduced by the kind of tracer (variability in staining intensity, background staining, tracer metabolism, tracer diffusion out of the axon) (Hayashi et al., 2007; Yu et al., 2015).

Immunohistochemistry is widely used to visualize MNs nowadays. However, even such a procedure does not guarantee the accuracy of MNs identification. In fact, primary antibodies commonly used to mark MNs are directed against antigens, such as SMI-32 (Carriedo et al., 1995, 1996; Morrison et al., 1998; Avossa et al., 2006; Martin et al., 2007; Blizzard et al., 2016; Biagioni et al., 2017), SMN (Dachs et al., 2013; Biagioni et al., 2017) or cholin acetyl transferase (ChAT) (Chang and Martin, 2011; Chopek and Gardiner, 2010; Ferrucci et al., 2010; Fayzullina and Martin, 2014), which are highly, but not exclusively, expressed by MNs. In detail, antibodies against SMI-32 recognize an epitope of a non-phosphorylated neurofilament heavy chain, which is quite ubiquitously expressed in the nervous system (Campbell and Morrison, 1989; Mesulam and Geula, 1991; Morel et al., 2002; Berglund and Ryugo, 1991; Straznicky et al., 1992; Carriedo et al., 1996; Fu et al., 2012). Accordingly, when SMI-32 immunohistochemistry was performed on spinal cord preparations, immune-staining unexpectedly included much more neurons other than MNs (Biagioni et al., 2017) (Fig. 2A). Similarly, SMN protein, despite being essential in MN survival

(Monani et al., 2000), is expressed much more ubiquitously than expected. The functions of SMN are not specific for MNs since it is a gem-associated protein involved in the biogenesis of small nuclear ribonucleoproteins and maintenance of spliceosome integrity (Martinez et al., 2012; Tsuiji et al., 2013; Maeda et al., 2014). Therefore, even in this case, the neuronal count uniquely based on SMN-immune-reactivity includes neurons other than MNs (Fig. 2B).

Finally, identification of MNs can be carried out by ChAT immunohistochemistry, although it is well-established that MNs are the main, but not unique, cholinergic population of the spinal cord (Fig. 2C). In fact, several ChAT-positive neurons are scattered throughout the grey matter, from the dorsal to the ventral horn, also including the Lamina X, around the central canal. In detail, apart from somatic MNs placed in the ventral horn, ChAT-positive neurons include: i) pre-ganglionic sympathetic neurons, within the intermediate/intermedio-lateral region; ii) partition cells and central canal cluster interneurons, within the Lamina X, which are components of the spinal motor network (Barber et al., 1991; Miles et al., 2007; Stepien et al., 2010); iii) dorsal horn neurons, scattered throughout Laminae III-IV (Phelps et al., 1990; Wetts and Vaughn, 1996; Gotts et al., 2016; Powis and Gillingwater, 2016); iv) dorsal commissural pre-ganglionic neurons, midline preganglionic cells forming an additional autonomic cell column in the spinal cord of rodents, which provide central control to pelvic adrenergic neurons (Hancock and Peveto, 1979). Remarkably, recent data demonstrate that a sub-class of the ChAT-positive spinal neurons other than MNs do degenerate in MN diseases (Nagao et al., 1998; Casas et al., 2013; Ruffoli et al., 2017), which further confuses the significance of ChAT immunohistochemistry to count MN integrity in the spinal cord.

In the light of these findings, it is evident that immunohistochemistry alone does not allow to discriminate MNs (Fig. 2). In fact, immunohistochemistry *per se* is not sufficient as a gold standard to assess stereological counts of MNs and the sole chance to identify spinal cord MNs is to combine immunohistochemistry with routine criteria. For instance, immunohistochemistry does not always stain MNs with the same intensity or within the entire cell body. In these cases, a nuclear

counterstaining (i.e with haematoxylin) might help to better define immunopositive neurons, allowing to count immunopositive cells which possess an evident nucleus.

The use of fluorophores to reveal the antigen-antibody reaction in immunohistochemistry sometimes allows to clearly identify MNs due to the enhanced contrast between the fluorophore, which positively stains MNs, and the darkness of the surrounding structures. When observed with confocal microscope it is possible to obtain a 3D reconstruction of MNs, which can greatly aid the counting procedure /be used to count. This technique allows to obtain very satisfying results in terms of single cell definition, but at the same time it does not give any information about the "context" within which the MNs are. Moreover, when not homogenously distributed in the cell immunofluorescence may cover cell contour reducing or enlarging the size of MNs. This calls for validating each specific immunofluorescence procedure both *in vitro* and most importantly *in vivo* by combining immunoperoxidase with immunofluorescence in pilot experiments in order to assess the pattern of immunofluorescence in each specific experimental condition, before carrying out an experimental analysis. For instance, when MNs are analyzed *ex vivo*, within the spinal cord or brainstem, it is important to also visualize the neighboring tissue, in order to evaluate MN number together with potential alterations of their topography or relationship with other cells as well as potential non-specific sources of fluorescence.

On the other hand, immunohistochemistry may positively rule out SBCs from MNs count since SBCs selectively express the 6A2 antigen, which characterizes the cell membrane of spinocerebellar neurons (Williams et al., 1990). Moreover, immune-reactivity for antigens specific for glutamatergic neurons, such as vesicular glutamate transporters, represents an additional, though less specific feature, which might contribute to distinguish SBCs from MNs.

The count of gamma-MNs in the context of MNs count deserves a dedicated discussion especially in the light of very recent data. Gamma-MNs are placed intermingled with alpha-MNs within the very same Lamina IX columns (Eccles et al., 1960; Willis et al., 1969; Bryan et al., 1972). They have morphological properties resembling those of alpha-MNs, with only slight differences

consisting of a smaller size, lower Nissl body density and lower number of synaptic contacts at the level of dendrites and cell body (Johnson, 1986; Martin et al., 2007; Pasquali et al., 2009). The smaller size of gamma-MNs remains the major distinctive feature between gamma- and alpha-MNs. In fact, in studies aimed at counting MNs both in normal subjects (Tomlinson et al., 1973, 1974) and in experimental MN disorders gamma-MNs are ruled out according to a size exclusion criterion (Martin et al., 2007; Fornai et al., 2008a; Ferrucci et al., 2010; Fulceri et al., 2012; Biagioni et al., 2017). Briefly, this consists in establishing a threshold size, which excludes neurons smaller than MNs from the neuronal count. This threshold value corresponds to neuronal diameters surpassing that of the widest gamma-MNs. If on the one hand it ensures to include in the count alpha-MNs which are in fact the biggest among all kinds of neurons, on the other, it may accidentally rule out some gamma-MNs as well. In any case, given the absence of totally specific features, the risk to include neurons other than MNs in MN count remains high if one does not exclude small neurons. For this reason, scientists felt more comfortable in reducing the total number of MNs by cutting off the number provided by those small gamma-MNs being below the threshold size. This point is relevant since it should prevent contamination of the MN count with other cell types, despite losing the pure quantitative number of MNs. Novel data produced in recent months led to reconsider such a correction in stereological counts of MNs since, as we shall see in the next paragraph, gamma-MNs may unexpectedly be refractory to MN disease, which selectively involves alpha-MNs instead (Lalancette-Hebert et al., 2016). Before we address this point comprehensively, a few considerations about the anatomy of gamma-MNs are necessary. Recently, a more specific characterization of gamma-MNs was achieved through the identification of antigens which are selectively expressed by gamma-MNs. For instance, it was found that, at the end of the CNS development, gamma-MNs down-regulate the neuronal marker NeuN and express a unique pattern of molecular markers, such as the glial cell line-derived neurotropic factor (GDNF) receptor Gfr-alpha1, the transcription factor Err3, Wnt7A, the serotonin receptor 5HT1d, and the alpha3 isoform

of the Na+/K+ ATPase (Friese et al., 2009; Shneider et al., 2009; Ashrafi et al., 2012; Enjin et al., 2012; Edwards et al., 2013).

Size-exclusion criterion provides the better parameter for MN identification. Again, this consists of including in the count only those MNs that possess a cell diameter higher than a threshold value, which represents the minimum cell size for considering a neuron as an alpha-MN. In this way, neurons which overlap in size with either gamma-MNs or cells other than MNs, are definitively ruled out, even if they satisfy the very same morphological criteria of MNs and are placed within the Lamina IX. According to this approach, gamma-MNs and small alpha-tonic MNs are not generally considered in the counts, thus leading to an underestimation of the authentic MN number. Again, following this procedure, MN cell count might be much more influenced by the amount of those MNs placed in the lateral extent of the ventral horn and innervating distal muscles, which are bigger in size, than MNs placed within the medial portion of the ventral horn and projecting to axial muscles, which are smaller in size and are likely to be ruled out from the count.

On the other hand, when a threshold cell (nucleus) diameter is established, care should be taken in order not to discard positive MNs. The size exclusion criterion allows to discard only those neurons with a total cell diameter (cytoplasm + nucleus) smaller than the established threshold value. This implies that MNs, which in the examined section do not exhibit their maximum diameter appearing below the threshold value, will be discarded. This affects the final number obtained in the count procedure, providing an underestimation of the total number of MNs, which indeed represents a limit of the size exclusion criterion. However, this counting approach is useful to avoid overestimation. This is the case of neurons other than MNs, such as SBCs, which would be erroneously included in the count otherwise. Underestimation which rules out mostly gamma-MNs does not produce dramatic effects since gamma MNs seem to be spared (Lalancette-Hebert et al., 2016). Thus, when the study is not aimed at obtaining an absolute number of MNs, but it compares the amount of MNs in wild-type/normal vs MN disease, then positive MNs are stochastically discarded in both experimental groups and this does not modify the ratio between the number of

wild-type and diseased MNs. In order to better define those neurons which might undergo an underestimation, one might use a complimentary IHC procedure allowing to include gamma-MNs. As previously reported, the most used antibodies for MN identification eventually stain even other neurons. In recent years, increasing efforts are being carried out in order to discriminate spinal neurons based on their specific antigen profile. This is the case of specific neurons, such as spinal border cells, which are positive for the 6A2 antigen, and gamma-MNs, which differentially express antigens such as NeuN, Gfra1 compared with alpha-MNs.

3.1 How motor neuron identity changes in pathological conditions

At this point, it is important to revise the criteria used to identify normal MNs when applied to MN disorders. This is a seminal experimental and pathological issue since MN count, apart from pure anatomical purposes, applies to MN disorders and specific physiological states. Remarkably, all disease conditions which cause MN death produce a variety of phenotypic changes within spared MNs. Sometimes these changes generate conflicting outcomes with those criteria commonly used to identify the same MN in baseline conditions.

For instance, changes in MN size commonly occur in MN disorders. Increased MN size is well documented following traumatic or glutamate-induced MN injury (He and Strong, 2000; Fulceri et al., 2011), and in experimental ALS, where both lumbar and brainstem MNs possess an increased cell diameter (Martin et al., 2007; Fornai et al., 2008a, 2008b; Ferrucci et al., 2010). Divergent results were reported in experimental Spinal Muscle Atrophy (SMA), where MN size was found either increased (Fulceri et al., 2012; Biagioni et al., 2017) or decreased (D'Errico et al., 2013; Powis and Gillingwater, 2016). This apparent inconsistency might depend on the different stages of a slow disease progression and the specific phenotype of SMA (ranging from a rapidly fatal disease to a disorder lasting several decades). In general, disease-dependent changes in MN diameter may sometimes be produced to cope with partial muscle denervation. This is expected to occur when disease progression is slow and the life span is long enough to allow compensatory responses to

occur (Fulceri et al., 2012; Biagioni et al., 2017). In contrast, in conditions of fast disease progression, when a massive MN degeneration occurs within a short time interval, the small size of remaining MNs might simply reflect the size of spared MNs (D'Errico et al., 2013; Powis and Gillingwater, 2016). Nonetheless, the nature of MN insult is expected to play a significant role since in the quick MN degeneration produced by a glutamate shot or trauma, MNs increase their size despite a short time interval.

Apart from size, MNs may change their shape becoming roundish in MN disease, which may be produced by a loss of descending activating pathways (Fornai et al., 2008a). In this case, the typical multipolar shape with clear cut dendritic branches is obscured by a generalized enlargement of the MN. Histochemical features vary as well in the course of MN disorders. Chromatolysis represents the prototype morphological alteration occurring in MNs after axonal or degenerative injury (Romanes, 1964; Lieberman, 1971; Wakayama, 1992). Such a chromatolytic reaction is well-evident in ALS MNs. In ALS, dying MNs are mostly characterized by vacuolar degeneration, consisting of cytoplasm dilution and loss of Nissl staining due to the occurrence of large, pale vacuoles filling the cytoplasm (Dal Canto and Gurney, 1997; Fornai et al., 2008a, 2008b; Ferrucci et al., 2010; Dziewulska et al., 2013). At electron microscopy swollen mitochondria, enlargement of granular endoplasmic reticulum, autophagy vacuoles and mitochondrial alterations are the main ultrastructural features occurring in ALS MNs (Menzies et al., 2002; Martin et al., 2007; Fornai et al., 2008a, 2008b; Pasquali et al., 2009; Ruffoli et al., 2015). Alterations in number, size, compartmentalization and morphology of mitochondria (i.e. swelling, matrix dilution and cristae derangement) may be measured using ultrastructural morphometry to characterize the various stages in MN life-span (Hervias et al., 2006; Martin et al, 2007; Fornai et al., 2008a, 2008b; Parone et al., 2013; Palomo and Manfredi, 2015). In particular, as recently demonstrated, mitochondrial damage in ALS occurs to different extents along disease progression depending on MN compartments, peripheral axons being the earliest and most severely affected with respect to cell

bodies and proximal axons (Natale et al., 2015). In contrast, during SMA, MNs typically appear hyperchromatic in H&E spinal cord preparations (Chou and Wang, 1997; Fulceri et al., 2012).

Even immunohistochemistry of MNs varies during disease conditions. For instance, a decreased ChAT immune-reactivity is reported in ALS MNs (Oda et al., 1995). This was supposed to be due to a loss of synaptic contacts (Ferrucci et al., 2010). This was recently confirmed by (Ramírez-Jarquín et al., 2014; Siembab et al., 2016) as the cause of a disconnection between MNs and Renshaw cells during ALS. In contrast, SMI-32 levels increase upon axonal damage (Tsang et al., 2000; Dziedzic et al., 2010; Harrington et al., 2010), and increased immune-reactivity for SMI-32 is found in SMA MNs, suggesting the occurrence of cytoskeletal alterations, which lead to neurofilament aggregation (Biagioni et al., 2017). Moreover, in SMA there is a massive causal loss of SMN protein which is the inherited cause of disease. Remarkably, this loss affects neurons other than MNs as well (Fulceri et al., 2012; Biagioni et al., 2017). Interestingly, although to a lesser extent, SMN protein is also altered in specific ALS, which indicates a commonality in disease mechanisms between different MN disorders (Tsuiji et al., 2013; Cauchi, 2014; Gama-Carvalho et al., 2017; Rodriguez-Muela et al., 2017; Singh et al., 2017).

Moreover, changes in MN site might also occur in MN disorders. This peculiar alteration was described in SMA patients by Simic and colleagues (2008), who demonstrated that in the spinal cord of children with fast progressing forms of the disease (namely, SMA-I and SMA-II) a significant number of MNs lie within the ventral white matter and even within the ventral roots. These misplaced MNs, referred to as heterotopic or ectopic MNs, were also described in SMA III (Fulceri et al., 2012), and are currently considered a pathogenic hallmark of the disease. MN misplacement in SMA is hypothesized to be due to abnormal migration of MNs being “attracted” by newly formed radial glial cells during development (Simic et al., 2008).

All these changes should be taken into account when counting MNs. For instance, increased MN size in ALS eventually leads to an underestimation of MN loss owing to a decreased threshold in the size-dependent exclusion criteria. This applies also to the fact that other MN subtypes (i.e.,

gamma-MNs, as well as small tonic alpha-MNs) may be included in the count. Since cell size is key in automated stereology, this should be corrected accordingly when normal or pathological MNs are counted.

Although at first glance such a limit of MN count may appear as a markedly weak point, some interesting recent findings reconcile the size-exclusion criteria with the specific pathology ongoing in MN disorders. In fact, the general concept that all classes of MNs are involved in ALS must be revised. Apart from the well-established finding that in MN disorders, and mostly in ALS, there is a relative sparing of MNs belonging to oculomotor nuclei, it is now ascertained that degeneration of tonic and phasic MNs does occur, although not homogeneously, but with a higher vulnerability of MNs innervating distal muscles. These MNs possess a large diameter, are placed in the lateral aspect of the ventral horn and appear to degenerate most in ALS (Tandan and Bradley, 1985; Pun et al., 2006; Nijssen et al., 2017). Moreover, recent experimental evidence indicates that alpha- and gamma-MNs undergo a completely different fate in MN disorders. In fact, it was demonstrated that small gamma-MNs are totally spared in ALS, where they produce a paradoxical disease-triggering role (Lalancette-Hebert et al., 2016) and in SMA, as well (Powis and Gillingwater, 2016).

In keeping with this, it appears that ruling out gamma-MNs and small tonic alpha-MNs does not diminish the power of analysis in detecting MN loss, but it rather represents a mandatory approach in order to document a disorder which naturally spares gamma-MNs and differently affects tonic and phasic alpha-MNs.

In addition, since expression of key proteins such as SMN, SMI-32 or ChAT is altered in pathological MNs, the chance to properly identify MN is reduced.

4. How to count motor neurons

Motor neuron number represents a hallmark to establish the pathology within spinal cord and brainstem in MN disorders.

Although neuroimaging is currently used in clinical practice and it is increasingly applied to investigate neurodegeneration in animal models *in vivo* (Zang et al., 2004; Niessen et al., 2006; Bucher et al., 2007; Waerzeggers et al., 2010; Evans et al., 2012; Kim and Song, 2013), this procedure does not possess the resolution required to visualize a single MN and it cannot be used to provide a quantitative evaluation of MNs in MN disorders. Therefore, the count of MNs *ex vivo* in the neuropathology unit, remains a seminal approach in order to assess MN loss, establish disease progression and evaluate the effects of treatments, which are tested to alter the disease course.

Motor neuron count is commonly carried out in sections prepared for light microscopy, and it can be performed trough two main procedures consisting of:

1- Direct cell count by the researcher

2- Automated stereology

Both these procedures are based on the correct identification of MNs, according to criteria reported above. However, as emerged from previous paragraphs, increasing technical approaches (and the increased insight about their limits) led, as a paradox, to complicate the positive identification of MNs. Therefore, it is not surprising that in order to infer correctly about the nature of a cell as a MN, it is mandatory to combine different procedures which take into account different (immunological and purely morphological) properties.

4.1 Direct count of motor neurons by the researcher

In the last decades, most studies aimed at providing MN quantification stem from a work published in the second half of the past century by Tomlinson and colleagues (Tomlinson et al., 1973). Impressed from the broad amount of data providing divergent results on MN number within the human spinal cord, these British neuropathologists established a methodological protocol to count

human MNs, with the purpose to guarantee suitable, consistent and reproducible data (Tomlinson et al., 1973). This protocol became a paradigm and it was applied by a number of investigators interested to quantify MNs in both humans and experimental models, under normal and pathological conditions.

In this work, the methodological procedure was carefully described step by step, beginning from fixation and isolation of the lumbo-sacral tract of the spinal cord, and subsequent identification, separation and embedding of each lumbosacral segment. However, as clearly realized by the authors, critical points were considered, consisting of: i) finding a correct procedure to collect the spinal cord sections; ii) establishing criteria to identify MNs; iii) counting MNs. Concerning the first point, different sampling procedures were compared. In detail, 20 μm-thick serial sections were obtained, and consecutively collected following a serial order; then, MN counts carried out in sections differently spaced along the whole lumbo-sacral tract were compared. On cresyl violet-stained sections, MNs were identified considering their size (ranging from 25 μm up to 80 μm), site (within the anterior horn, and specifically in the lateral group, since they are interested in counting only MNs which supply lower limb muscles), and shape (multipolar cell body with densely-stained Nissl substance, central nucleus and a well-evident nucleolus). Occasional occurrence of large neurons, very similar to but other than MNs, as well as the presence of gamma-MNs, very close to alpha-MNs but smaller in size, were also pointed out. Finally, MN population within the lumbo-sacral tract of the spinal cord was quantified by counting nucleoli and data obtained following different sampling procedures were analytically compared (Tomlinson et al., 1973).

Tomlinson's procedure was used in a variety of studies as the reference method to quantify MNs in human subjects (Tomlinson et al., 1974; Tomlinson and Irving, 1977; Kawamura et al., 1977; Cruz-Sánchez et al., 1998; Stephens et al., 2006; Ravits et al., 2007). However, taking into account the highly conserved cytoarchitecture of the spinal cord in mammals, an adapted form of the Tomlinson's procedure was actually applied as the most reliable method to count MNs also in experimental models. For instance, in the very same months in which Tomlinson and colleagues

were developing their protocol, Papapetropoulos and Bradley used Tomlinson's procedure to count MNs within the spinal cord of animal models of muscular dystrophy and SMA. These authors, who referred to Tomlinson's procedure before it was actually published, stated that identification of MNs in these animal models was more difficult than in human subjects, since "[…] in the mouse, the ventral horn motor neurons are not as clearly demarcated from other neurons as in man" (Papapetropoulos and Bradley, 1972). For this reason, the authors modified Tomlinson's procedure, in order to adapt some criteria to their experimental conditions. For instance, based on cresyl violet staining, neurons were classified in three arbitrary groups (I- neurons with extremely dense Nissl substance, II-neurons with dark prominent Nissl substance and maximum diameter equal or greater than 25 μm, III-all remaining neurons), and separately counted. Accordingly with Tomlinson's procedure, only neurons with evident nucleoli were counted, while differently from Tomlinson's procedure, thickness of the slices was reduced (10 μm), and size and site criteria were disregarded (Papapetropoulos and Bradley, 1972). Therefore, despite the huge effort to provide a systematic quantification of the ventral horn neurons (overall, more than 80,000 sections were used!), the lack of a systematic experimental protocol reduced the scientific relevance of the results obtained.

Starting from these pioneer studies, literature about MN count in a variety of experimental models of MN disorders increased over the years. In these studies, counting procedures share general items, such as (i) collecting serial sections, (ii) identifying MNs, and (iii) counting MNs using an appropriate magnification under light microscope, but they differ from each other concerning the implementation of specific experimental steps. For instance, thickness of the slices as well as sampling procedure, which in turn influences the total amount of slices used for the counts, are variable. However, concerning MN identification, morphological criteria are quite homogeneous. In fact, on the basis of their peculiar morphology (i.e., multipolar shape, prominent nucleolus, and Nissl granules broadly scattered in the cytoplasm) MNs are almost exclusively identified in cresyl violet- or H&E-stained histological preparations (Rende et al., 1992, 1993, 1995; Morrison et al., 1998; Martin et al., 2007; Barbizan and Oliveira, 2010). Similarly, size exclusion criterion appears

to be constantly applied. Interestingly, whenever the aim of the study is counting alpha-MNs, a wide agreement among different authors exists concerning the utility to adopt a size exclusion criterion which allows to rule out the small gamma-MNs (Tomlinson et al., 1973; Johnson, 1986; Ishihara and Araki, 1988; Carriedo et al., 1996; Stephens et al., 2006; Martin et al., 2007; Fornai et al., 2008a, 2008b; Chopek and Gardiner, 2010; Ferrucci et al., 2010; Fulceri et al., 2012; Biagioni et al., 2017). However, differences among authors occur concerning the threshold value considered to discriminate alpha-MNs. In general, when applied to rodents, a cell diameter $\geq$ 20 μm represents the most common cut-off to selectively count alpha-MNs and rule out at the same time a large part of the gamma-MN population (Schaffner et al., 1987; Carriedo et al., 1995, 1996; Avossa et al., 2006). Other authors brought this limit up to 30 μm in the mouse spinal cord (Martin et al., 2007; Fornai et al., 2008a, 2008b) while Tomlinson and colleagues established a cut-off value of 45 μm to reasonably rule out a wide percentage of gamma-MNs in the human spinal cord (Tomlinson et al., 1973).

Most authors merely refer to MNs as neurons placed within the ventral horn (Papapetropoulos and Bradley, 1972; Rende et al., 1992; Morrison et al., 1998; Ciavarro et al., 2003; Martin et al., 2007; Suzuki et al., 2007), others consider their site within the dorsolateral division of the ventral horn (Tomlinson et al., 1973; Irving et al., 1974), or again, more specifically, within Lamina IX (Barbizan and Oliveira, 2010). This scarce use of a systematic topographic criteria for identifying MNs is probably due to the fact that morphological and size exclusion criteria actually guarantee to include in the count a very large MN population, and the application of a further parameter might be considered superfluous. However, far from being an arbitrary parameter, MN site is required to reduce ambiguity in MN identification. This is even more crucial for brainstem MNs, which lie in the motor nuclei and send their axons within the cranial nerves. In fact, in this case MN identification essentially consists of identifying motor nuclei within the brainstem (Haenggeli and Kato, 2002b; Lladó et al., 2006; Lever et al., 2009). This might be achieved through an in depth

analysis of those brainstem structures (nuclei, fasciculi), which are topographically related with each specific motor nucleus. This procedure can take advantage of specific brain atlases, which report detailed descriptions of the structures that are evident in each consecutive brain section, referred to as stereotaxic coordinates. However, in these studies, MN size and morphology are indeed used to discriminate alpha- and gamma-MNs, since it is generally supposed that brainstem motor nuclei contain exclusively MNs.

4.2 Counting motor neurons through automated stereology

Stereology consists of a mathematical-based procedure which allows to obtain estimation about global quantities of specific objects (cells, fibers, synapses) occurring within a region of interest, which possesses specific size, area, and volume. Therefore, stereology allows to provide quantitative three-dimensional information starting from two-dimensional observations.

A prodrome of stereological method was elaborated by Abercrombie (1946), who defined the ‘‘profile counting’’ as the 2D count of each specific structure occurring within equally spaced thin sections. In the effort to obtain reliable measures by counting only a few sections, Abercrombie produced a counting correction formula, namely “Abercrombie’s formula”, which allows to correct for overcounting. In fact, this mathematical formula adjusts the final number obtained by counting objects within serial sections by using factors, which take into account the thickness of the sections and the size of the objects counted. Since then, technical progress in light microscopy together with the development of stereology software has taken place. However, a reliable sampling procedure still represents a major point even in stereology-based counts.

Stereological methods are classified in “assumption-based” or “model based” or “two-dimensional (2-D)” approaches, and “design-based” or “three-dimensional (3-D)” approaches, these latter also called “unbiased” methods.

In the “assumption-based” 2-D stereology, the fundamental assumption consists of considering that objects to be counted possess the very same shape, size, spatial orientation and frequency

throughout the whole anatomical region to be analysed. This method was commonly used for a long time to measure the total number and the density of objects within a specific region by counting only a sample of the total sections of the entire region of interest (Weibel and Gomez, 1962; Konigsmark, 1970). This approach suffers from a gross approximation when applied to biological structures, which indeed possess inconstant and irregular features. For instance, when 2-D stereology is used to count MNs, some concerns arise when cells under investigation exhibit different morphometry due to physiological variability (see, for instance, the wide range of size exhibited by different groups of MNs), or following pathological processes. This generates bias, only partially corrected by using algorithms, such as the above reported Abercrombie's formula.

In the last decades, great efforts were made to minimize the source of potential bias in stereology, due to the high discrepancies between the theorized (ideal) and actual (real) features of biological structures. This yielded the development of alternative stereological procedures, called "design-based" or 3-D stereology, which allow to analyse volume, number and densities of objects within a specific region, and also provide information about the spatial distribution of the objects throughout the region of interest. The term "design-based" indicates that the methods and sampling procedures are "designed", that is, are independent from the size, shape, spatial orientation, and spatial distribution of the objects (i.e. cells) to be investigated (West, 1999, 2002; Schmitz and Hof, 2005, 2007). This method is also indicated as "assumption-free", since it does not employ any assumption, which might predictively model the objects under investigation. Again, design-based stereology is also referred to as "unbiased stereology", since it is grounded on statistical sampling procedures and spatial randomness of the objects.

Through design-based stereology, objects might be counted by using the "physical disector" or simply "disector" (namely "two" (di-) "sections") method, which allows to count objects within a couple of adjacent sections. By applying specific criteria, this method allows to identify and count the objects within a specific field occurring in both sections analyzed. As an extent of the disector method, the "optical disector" method consists of creating different focal planes through the section.

In this method, two sections are analyzed: one is the reference section, which corresponds to the focal plane, the other is the lookup section, which is immediately above the focal plane. Objects that are visible (in focus) only within the reference section are countable, whereas objects that are in focus within the lookup section (and then also visible in the reference section) are ruled out. In the case of large numbers of total objects to be counted, 3-D stereology resorts to additional sampling methods (i.e. the "physical fractionator" or the "optical fractionator" methods), in order to provide an estimate of the number of objects occurring within a specific region. Therefore, while the optical disector allows to count objects within samples with a specific thickness, the optical fractionator allows to refer the measure obtained within a "sample" to the entire volume of the region under investigation (Sterio, 1984; Braendgaard and Gundersen, 1986; Gundersen, 1986; West et al., 1991; Cruz-Orive, 1997; 2004; West, 2012a; 2012b).

A number of additional technical methods (probes) and specific algorithms (estimators) were developed in these last decades leading to an increasing improvement of 3-D stereology. Among these, it is worth mentioning Cavalieri's formula, which allows to estimate the volume of specific regions, and the Horvitz-Thompson estimator, used to estimate the number of objects which are stratified within a specific region. Other specific methods to measure volume, number, and densities of objects, as well (i.e. optical rotator, nucleator, etc.) allowed 3-D stereology to be applied in a wide range of studies.

4.2.1 A step-by-step protocol of design-based stereology to count motor neurons

In the present paragraph a protocol to count MNs in the lumbar spinal cord of the mouse through a design-based stereology with the optical fractionator probe is reported (Battaglia et al., 2015). This procedure is performed using a Zeiss Axio Imager M1 microscope equipped with a motorized stage and focus control system (Zeta axis), and a digital video camera. The software Image-Pro Plus 6.2 for Windows (Media Cybernetics, Inc., Bethesda, MD) equipped with a Macro (Immagine and Computer, Bareggio, Italy; King et al., 2002) is used for the analysis of digital images.

In detail, mouse spinal cord is dissected out and fixed with Carnoy's solution, consisting of 60% ethanol, 10% acetic acid, 30% chloroform. This step induces a 30% reduction in the length of the spinal cord, which should be taken into account when selecting the specific spinal tract to analyse (for instance, the length of the lumbar tract is about 6.5 mm and it is reduced to 4.5 mm after fixation). The lumbar tract is isolated by cutting the spinal cord into three blocks corresponding to cervical, thoracic and lumbar tract, using as reference points the enlargement (defining the cervical and lumbar tracts) and constriction (for thoracic tract) visible along the cord. Twenty μm-thick serial sections are cut and collected every 100 μm (one out of 5 sections). In these sections anti-SMI-32 immunohistochemistry is carried out to label MNs (Fig. 3A).

In this way, the number of SMI-32-positive MNs is assessed in about 40 sections out of a total of 200 sections obtained from the whole lumbar spinal cord. Each section is analysed along the horizontal axis and MNs belonging to medial and lateral columns of the ventral horn are identified and outlined at 2.5 X magnification. In detail, a grid of disectors (grid size 150 μm X 150 μm) with 1.3 as numerical aperture of the lens is used (Fig. 3B). Within counting frames of 40 μm X 40 μm, SMI-32-positive MNs with a cell body diameter > 30 μm are counted at 100 X magnification, as described (Gundersen and Jensen, 1987) (Fig. 3C). The total number of MNs is computed by using the formula:

$N = \Sigma(n) \times 1 / SSF \times 1 / ASF \times 1 / TSF$

where: n = total number of cells counted on each disector; SSF (sampled sections fraction) = number of regularly spaced sections used for counts divided by total number of sections across the lumbar spinal cord (in the representative sections and calculations provided here, corresponding to 1/5, since 1 out of 5 slices - i.e, 40 out of 200 slices - were used for the count); ASF (area sampling frequency) = the disector area divided by the area between disectors (here corresponding to 1600 μm^2 x disector number/region area); TSF (thickness sampling frequency) = disector thickness divided by section thickness (here corresponding to 16 μm/20 μm).

This procedure was used to count the number of MNs in experimental ALS. According to Fornai et al. (2008a), the threshold value for the MN cell body diameter in ALS mice was increased by 7% compared with wild type mice, thus reaching 32.1 μm (Fig. 4). This correction in the cut off threshold in normal versus diseased conditions was obtained by referring to H&E-stained sections, which (as stated previously) allows to correctly measure the cell contour of MNs.

4.2.2. Limits for the use of automated stereology in motor neuron count

In general, unbiased stereology provides more accurate, precise, and reproducible data, thus significantly reducing bias, and providing important advances compared with the classical methods (Benes and Lange, 2001; Schmitz and Hof, 2005, 2007). Together with increasing technical progression in light microscopy, design-based stereology represents nowadays the most common procedure to quantify neuroanatomical structures, such as fibers, dendritic spines, and neurons as well (Braendgaard and Gundersen, 1986; Mayhew, 2014; Wang et al., 2014; Golub et al., 2015). On the other hand, as described above, unbiased stereology allows to extend to the entire region of interest the data obtained by counting objects within small samples. Such a sampling procedure, despite being time-saving, provides unbiased results only when objects (i.e., cells) are randomly distributed within the whole region of interest. This rarely occurs in the CNS, where generally neuronal structures, such as neurons or synapses, do not possess a stochastic spatial distribution. In contrast, within specific CNS regions, such as the spinal cord, MN localization within the ventral horn is widely variable, depending on specific somatotopy. These conditions may create bias in 3-D stereology, leading to a paradoxical contradiction of its virtually unbiased definition.

Although several studies used design-based stereology to count MNs within the brainstem (Nimchinsky et al., 2000; Wiggins et al., 2012; Faunes et al., 2016) and the spinal cord (Morrison et al., 1998; Martin et al., 2007; Saxena et al., 2007), the number of studies where MNs are directly counted by the researcher at light microscopy, both in normal and pathological conditions, appears predominant in literature (Azzouz et al., 2000; Haenggeli and Kato, 2002b; Chi et al., 2006; Lladó

et al., 2006; Stephens et al., 2006; Ravits et al., 2007; Fornai et al., 2008a; Ferrucci et al., 2010; Dachs et al., 2011; Fulceri et al., 2012; Yoo and Ko, 2012; Biagioni et al., 2017). These findings suggest that, when counting MNs the role of the researcher, who should identify and count MNs in consecutive sections by applying specific criteria, is generally preferred over completely automated procedures. In support to this claim, Ravits and colleagues' findings argued against the suitability of stereology technologies in MN quantification as well as against the efficiency of automated particle counting software (Ravits et al., 2007). Such a pitfall might depend on several reasons. For instance, the lack of randomization in the spatial distribution of MNs makes the small sample size used in 3-D stereology inadequate to provide reliable data about MN number. In fact, the complex cytoarchitecture of the ventral horn, where MNs and other neuronal populations are closely intermingled with spatial relationships, varies along different tracts of the spinal cord. This requires additional criteria, which impairs stereological automatisms. The intrinsic variability of MN density becomes critical in the presence of pathological processes, which cause different patterns of MN loss along the spinal cord. Again, in MN disorders a significant change in MN size is reported (Martin et al., 2007; Fornai et al., 2008a; Simic et al., 2008; Fulceri et al., 2012). This concept leads to a critical point when applied to the 3-D stereological count of MNs. In fact, in the presence of MN disorders the increase in MN size affects MN identification when it occurs under rigid stereological coordinates, which assign to the counting software a specific threshold diameter in order to include MNs solely. For instance, MN enlargement along diseased CNS causes a shift in MN size which leads to recruit as "stereologically defined MNs" neurons other than MNs. This occurs differently in control subjects, which necessarily leads to underestimate the amount of MN loss.

In the light of these considerations, it is conceivable that unbiased MN count might actually result from integration of different techniques, which include confocal microscopy, electron microscopy, and design-based stereology, as well (Schmitz and Hof, 2005).

5. The stereology-like procedure as a new method to provide unbiased motor neuron quantification

In this section, we report the protocol of a stereology-like procedure to count MNs, which combines specific technical devices (aimed at collecting sections and identifying MNs) with direct cell count at light microscopy.

The stereology-like procedure essentially combines dimensional, topographical and morphological criteria (namely size, site and shape) with *ad hoc* sampling procedure (i.e., collecting sections), in order to minimize counting errors and provide reproducible data. Like the classic stereology, the stereology-like procedure quantifies structures occurring within serial sections observed under the light microscope. Like design-based stereology, systematic criteria are used to make the measure "unbiased". However, the stereology-like procedure is unique since it does neither require correction formulas nor technologically advanced equipment (sophisticated technical instruments or advanced image analysis software).

This procedure was devised in our lab, when we investigated MN disorders. Using this procedure, we were able to quantify MNs in control and diseased spinal cord, and associate MN loss with motor impairment at defined disease stages. In these models, the stereology-like procedure allowed to count MNs within the whole lumbar (Fornai et al., 2008a; Ferrucci et al., 2010; Fulceri et al., 2012; Biagioni et al., 2017) and cervical tract (Fornai et al., 2008a) of the spinal cord, and within the brainstem motor nuclei (Fornai et al., 2008a; Ferrucci et al., 2010). Moreover, this procedure allows to provide quantitative evaluation of the effects of a chronic treatment on MN survival, thus resulting in a useful tool to estimate the efficacy of potential therapeutic strategies (Fornai et al., 2008a; Ferrucci et al., 2010; Fulceri et al., 2012; Biagioni et al., 2017).

The stereology-like procedure consists of three phases: 1) sample preparation; 2) sampling procedure; 3) MN identification and count.

1) Sample preparation. Our protocol plans to embed brain and spinal cord samples in paraffin, after fixation by 1 M phosphate buffer containing 4% paraformaldehyde. Fixation of brain and spinal

cord starting from *in vivo* models requires the choice of the appropriate fixing procedure, consisting of perfusion followed by immersion of samples within the same fixing solution for 24 hours. This is critical in order to preserve neuronal morphology, minimizing the risk of *post-mortem* artifacts. This fixing procedure also allows to simplify brain and spinal cord dissection from the skull and the vertebrate column, respectively, avoiding errors due to a mechanical damage. Different regions of interest along the spinal cord (namely, cervical, thoracic or lumbar tract) are embedded, whereas the brain is embedded as a whole.

To correctly identify the single segments of the spinal cord, the emergence of spinal nerves represents the gold standard to establish precisely the spinal cord tracts.

Nonetheless, when the spinal cord is already dissected out from the column, it might become difficult to maintain the correspondence between nerve emergence from the cord and vertebral column. In fact, in this experimental phase, nerves can be cut or torn up during bone removal. Therefore, in this case, visualization of the cord enlargements might represent a good reference allowing to easily recognize both the cervical and the lumbar tract of the spinal cord.

Alternative procedure by immersion in Carnoy's fixing solution might be peformed (see previous 4.2.1 section). In fact, Carnoy's solution is often used as an alternative fixing solution to buffered paraformaldehyde-containing solutions. It is routinely used in surgical pathology, when tissues are dissected out and immediately fixed before histochemical or immunohistochemical procedures. An extensive study, which compares different fixing solutions in order to obtain an optimal preservation of tissue architecture and cell morphology, demonstrates that Carnoy's solution shows good results when applied for relatively short times (i.e. 6 hours) compared with formalin solution (which needs 24 hours or more), whereas formalin-fixed specimens are qualitatively superior when staining, nuclear and cellular shrinkage, distortion or dissolution are evaluated (Singhal et al., 2016). Another study, which compares specimens from colorectal cancer fixed with formalin or Carnoy's solution, shows that both fixing methods guarantee a comparable preservation of cellular and molecular morphology (Pereira et al., 2015). Therefore, in some experimental conditions, i.e.

when a high number of samples should be analyzed, and the sample size is small, fixing with Carnoy's solution represents a good tool to preserve tissue quality while saving time (the smaller the size of the specimens the less time is required for the fixing solution to penetrate in depth). On the other hand, classic perfusion remains the ideal fixing procedure, which is preferentially used in stereology-like procedure, since it allows perfusing fixative to quickly reach every cell of the entire organism via the vascular system, where it circulates pushed by a peristaltic pump at an appropriate pressure. This fixing procedure also allows to minimize the time interval between the death of the animal, the onset of post-mortem changes, and sample dissection, and it is recommended in *in vivo* experiments, when the tissue/organ of interest can be dissected from a whole organism, where the circulatory system gradually passes from driving blood to conveying the fixing solution. Anyway, perfusion requires a lot of time and a volume of fixing solution far higher than fixation by immersion (approximately 30 minutes and about 150-180 ml for a single mouse). In a perfused animal, tissues of interest should be dissected out and post-fixed by immersion in the same fixing solution, in order to obtain a good morphology (i.e., for paraformaldehyde-containing solution a post-fixation of at least 24 hours is recommended). Again, perfusion precludes the possibility to use the tissue for any assays other than morphological procedures (namely, biochemical assays).

After fixation, paraffin-embedded samples are preferred, because of easier handling. Paraffin-embedded samples, each containing the region of interest, are entirely cut by microtome, in order to obtain 7/8 μm-thick sections. Thickness of the sections is an important parameter. In fact, the optimal thickness of the sections is critical in order to correctly visualize neurons, fibers, and other CNS structures. Slice thickness exceeding 10 μm markedly worsens sharpness and resolution of the pictures, thus impairing MN identification (Fig. 5).

Inclusion of the tissue into a block of paraffin allows to easily handle the specimen, which can be sectioned immediately or stored for later usage. Moreover, the lower thickness of sections obtained from embedded tissue blocks compared with that of unembedded vibratome-sectioned tissues, allows to better observe more morphological details. However, embedding in paraffin affects the

size of the tissue, which might be avoided by directly cutting perfused nervous tissue using a vibratome. Therefore, when quantitative morphology is performed, tissue shrinkage represents a bias and a correction factor is required to adequately correct the size changes caused by the embedding procedure. On the other hand, this correction factor does not represent a constant value but may vary depending on the CNS matrix (trim with its specific biophysical properties). Thus several issues determine the extent of tissue shrinkage, such as duration of the fixation and dehydration, beyond tissue composition. For instance, concerning the nervous tissue, different neuroanatomical regions show different shrinkage, the brainstem shrinkage appearing less pronounced compared with the forebrain, mainly depending on white and grey matter composition, water content, etc. (Ogata and Feigin, 1973; Kretschmann et al., 1982; Quester and Schröder, 1997). 13% or 10% represent an average correction but the ideal corrections should be applied according to the specific experimental conditions. Again, a correction of 30% is required when nervous tissue is fixed by immersion in Carnoy's solution. For this reason, special care should be taken in evaluating the amount of shrinkage produced by different methods within comparable segments of the CNS.

2) Sampling procedure. Sampling procedure consists of selecting sections, which should be used for the counts among the total amount of sections collected for each sample. Sampling procedure is determined by two parameters: thickness of the sections, and size of the structures (i.e. MNs) which are to be counted. In detail, the distance between two consecutive sections should be high enough to avoid double counting of the same structures, but low enough to maximize the count within the sample. This gets complicated by the fact that specific biological structures do not exhibit a unique size, but rather possess a size range, which is often shared with other different structures. Therefore, sampling procedure should select sections at a distance, which corresponds to the highest size possessed by the structures to be counted. In this way, double counting of the same structure is completely avoided, although smaller structures, occurring within the discarded sections, are lost, leading to underestimate the total number obtained.

For instance, in the stereology-like count of MNs in a mouse model of ALS, we collected serial, consecutive, 7-8 μm-thick sections of lumbar spinal cord and we counted MNs in every tenth section, spaced 80 μm (resulting from 10 x 8 μm) (Fig. 6A). This sampling procedure was carried out based on previous literature, where the maximum MN diameter within the lumbar spinal cord was estimated at 60-65 μm (Martin et al., 2007). Thus, the 80 μm distance between two consecutive sections allowed us to count distinct MNs in different slices (Fornai et al., 2008a).

When the maximum diameter of MNs changes, then distance between sections used for the count should be modified. This condition occurred when we counted MNs within brainstem motor nuclei. In fact, since the maximum brainstem MN diameter is estimated around 50 μm, MN counts were carried out in consecutive sections spaced about 50 μm (i.e. every seventh 7-8 thick sections, Ferrucci et al., 2010) (Fig. 6B). Again, a maximum MN diameter of 60 μm is found in the SMA-III model FVB/NJ mice (a different strain mouse compared with C56Bl mice, which is the strain of transgenic mice used as ALS model) due to the documented strain-dependent variability of neuron size (Penet et al., 2006; Fulceri et al., 2012). Accordingly, in this study the distance between two consecutive sections where motor neurons were counted was reduced to 60 μm (Fulceri et al., 2012; Biagioni et al., 2017).

3) Motor neuron identification. In the stereology-like procedure, identification of MNs requires combining different parameters: a) shape and histochemistry, b) size, and c) site of MNs.

a) To this purpose, H&E is the most appropriate histological staining. In fact, the dual acidophilic and basophilic properties of such a common histochemical staining allow to highlight MNs within the spinal cord and/or brainstem tissue (Fig. 1A). In fact, H&E offers a good contrast between the intense basophilic cytoplasm, the pale basophilic nucleus and the acidophilic extracellular matrix. This allows to easily identify the borders of both cells and nuclei. As an alternative, basophilic cresyl violet, tyonine or toluidine blue staining, by binding to acidic molecules, which are abundant in MNs due to their high content in nucleic acids, can also provide an appropriate MN visualization

(Figs. 1B, 1C). However, the lower contrast provided by cresyl violet or toluidine blue might not allow to clearly define MNs. For these reasons, in our stereology-like count we prefer to use H&E-stained sections, deserving cresyl violet or toluidine blue as alternative (not preferential) staining procedures.

b) However, as widely discussed in a previous paragraph, morphological criteria are not sufficient for a proper MN identification. In our stereology-like protocol, we also referred to the MN size and site. In particular, once a potential MN is identified at low magnification (4 X or 10 X), the maximum and minimum diameter of the cell body should be measured at increased magnification (20 X) and the MN diameter ("size") of the cell body is calculated as the resulting mean value (Fig. 7). Measure of MN diameter can be obtained directly at the microscope by using current image analysis software, or applying freely downloadable NIH ImageJ software on captured images. At this point, the size exclusion criterion must be applied. This consists of setting a minimum threshold size, namely the "cut-off", which allows to rule out smaller sizes. In this regard, it is important for the researcher to be aware that a few MNs might not be included in the count since their maximum diameter may not be appreciated, being differently oriented compared with the slicing planes of the sections under observation. However, this intrinsic bias becomes negligible in modifying the final result, since the probability to rule out true MNs is the same in each experimental group. Our procedure, instead of offering a method to obtain absolute numbers, has been conceived as a handy, "basic" method, which does not require the use of sophisticated instruments but allows to evaluate the extent of MN degeneration in MN disease using equipment which is routinely present in each lab for morphological studies.

Size exclusion criterion must vary depending on MN size differences occurring through spinal cord and brainstem motor nuclei (Fornai et al., 2008a; Ferrucci et al., 2010; Fulceri et al., 2012; Biagioni et al., 2017). For instance, it is well-known that brainstem MNs are generally smaller than spinal cord MNs. Accordingly, we modified the size exclusion criterion relative to the MN size. Thus, within the cervical and lumbar spinal cord of ALS mice, size exclusion criterion was established at

30 μm, also in line with the paper by Martin et al. (2007), where MN diameter of the cell body was considered ranging from 30 μm to 45 μm (Fornai et al., 2008a; Ferrucci et al., 2010). This cut-off value is not feasible within brainstem motor nuclei, due to both the general smaller size of the brainstem MNs' cell bodies compared with those in the spinal cord and the high variability in MN size between different brainstem nuclei. In fact, within the brainstem, some motor nuclei, such as trigeminal, facial, and hypoglossal nucleus, possess a highly heterogeneous MN population (Ferrucci et al., 2010). In particular, MN cell body diameter ranges from 15 μm (except for the smallest MNs found within the facial nucleus, which can measure even 5 μm) to 50-55 μm. In these conditions, the size exclusion criterion was extended to include even smaller MNs up to 15 μm diameter (Ferrucci et al., 2010) (Fig. 8).

As stated above, MN cell body diameter also varies in different strains of mice (Penet et al., 2006). Therefore, when MNs were counted in FVB/NJ mouse strain, used for producing SMA models, size exclusion criterion was established at 22 μm, due to the smaller MN diameter of FVB/NJ compared with C56Bl mice, used for producing ALS models (Fulceri et al., 2012; Biagioni et al., 2017).

Moreover, aging alters MNs' cell body size and number (Hashizume et al, 1988; Hashizume and Kanda, 1995; Zhang et al., 1996; Matsumoto, 1998; Schwarz et al., 2009; Webber et al., 2009), thus making it necessary to modify the cut off value accordingly.

On the other hand, some flexibility in applying threshold values to identify MNs is required if one considers that measurements of MN cell bodies may vary also depending on the specific software used for determining MN size. For instance, in the abovementioned study by Martin and coll. (2007), carried out in ALS mouse models, the optical disector method was used for identifying and counting MNs on the basis of morphologic and size exclusion criteria, and image analysis combined with the Inquiry software (Loats Associates, Westminster, MD) were also used in order to determine MN areas. A different method was applied by Fornai et al. (2008a) in the study on ALS mice, where the neuronal diameter and area were measured by image analysis software (Molecular

Machine & Industries AG), which allowed drawing the cell body diameter or delineating the cell contour under observation and automatically reading the related numerical values. The same software was also used for measuring the cell body diameter of brainstem MNs in ALS mice by Ferrucci and coll. (2010), as well as in SMA-III mice models analysed in the study by Fulceri and coll. (2012) and Biagioni and coll. (2017). Again, MNs counted in ALS patients by Ravits and coll. (2007) were identified based on morphological and size criteria, both evaluated at light microscopy equipped with Spot Insight 4 digital camera and Spot Advance version 4.5.7 software (Diagnostic Instruments, Inc., Sterling Heights, MI). Other authors, performing automated stereology, used the optical fractionator technique (i.e., Morrison et al., 1998, in a mouse model of ALS) or the physical disector method (i.e. Simic et al., 2008, in humans affected by SMA) to determine MNs number and morphometry. Given such a high variety of measurement procedures, it is crucial that each author describes carefully the specific technique and/or instruments used for the morphometric analysis in order to make reliable comparisons between data obtained by different methods. Finally, due to the pathological enlargement of MN cell body diameter, which is well-documented in MN disorders (Martin et al., 2007; Fornai et al., 2008a, 2008b; Fulceri et al., 2012; Biagioni et al., 2017), it is very likely that several small MNs, that are not counted in controls, might be included in the count in diseased mice. On the other hand, restricting MN quantification to phasic alpha-MNs does not reduce the suitability of the final results. In fact, it is now well-documented that the pattern of MN degeneration in ALS shows an increased vulnerability of phasic alpha-MNs, which are affected earlier than tonic alpha-MNs (Nijssen et al., 2017).

Moreover, recent evidence indicates that MN pathology spares gamma-MNs (Lalancette-Hebert et al., 2016; Powis and Gillingwater, 2016).

c) Another criterion required to identify MNs refers to the specific localization of MNs within the grey matter of the spinal cord and brainstem. This is a site-specific criterion, which allows to identify the exact area within which MN counts should be carried out.

In the spinal cord, depending on the level, this area corresponds to one up to three specific columns, each one representing Rexed's Lamina IX. Namely, in the cervical and lumbosacral enlargements the columns are three (Rexed, 1954). The use of Atlas of brainstem (Watson et al., 2009) and spinal cord (Paxinos and Franklin, 2004) is mandatory (Fig. 8). For instance, Atlas tables were used to identify the medial, intermediate and lateral MN columns within the mouse spinal cord (Watson et al., 2009), where MNs were counted separately, in order to obtain distinct counts for MNs innervating axial muscles, and MNs innervating proximal and distal limb muscles (Fulceri et al., 2012). Using Atlas tables as reference, it is helpful to draft the border of those areas where MNs should be identified (Fig. 8). The border of MN pools varies depending on the various segments of the spinal cord and may differ from the border of lamina IX as generally provided by each specific atlas. Thus, an in depth evaluation encompassing multiple methodologies should be applied as a preliminary step to assess specifically where to count. This is especially true for the intermediate and medial MN columns, whereas the lateral MN column is generally more defined. This might explain why studies, which do not refer in a systematic manner to MN topography, perform MN counts within the lateral portion of the ventral horn (Thomlinson et al., 1973; Irving et al, 1974; Stephens et al., 2006). Therefore, once the MN area is identified, applying size and histochemical criteria is mandatory.

The entire stereological-like procedure is summarized within the drawing of Fig. 9.

In the stereology-like procedures the total amount of MNs counted within a specific tract of spinal cord results from the arithmetic sum of MNs counted in each section analysed.

At this regard, the generalized formula is applied:

$N = d/ns \sum x$

where: N = total estimated number of cellular bodies; d = length of the rostrocaudal axis of the segment or region being assessed; n = number of non-contiguous slices counted per segment or region; s = thickness of the section; x = number of perikarya counted per non-contiguous slice. This formula though being valid when applied under controlled experimental conditions, provides an

approximation of the "real" number of neurons occurring within a certain ROI. In fact, the final number N becomes representative of the actual neuron number only when the number of sections analyzed is high enough to give ns = d. Indeed, this equivalence cannot be obtained and it represents an asymptote, which approximates the biological reality. On the other hand the use of a mathematical formula depends on the ability to obtain a number which exactly quantifies a biological condition. In fact, the previous generalized formula assumes that in all sections of the ROI (even in those that have not been included in the count) the number of neurons is always the same, and it corresponds to the number of neurons which has been actually counted in a definite number of sections. In some conditions, this might be acceptable and the final result might represent a good approximation of the true value. In any case, in the spinal cord the topographic distribution of MNs changes even within the same nucleus, and this becomes unpredictable especially when MNs are analyzed in diseased conditions, which alter *per se* the normal architecture of the nucleus. This high variability in the spatial distribution of MNs reduces the reliability of any algorithm. The stereological-like procedure provides quantifications, which are not "adjusted" or "corrected", but derive from a broad sum of the neurons actually counted within a high number of analyzed sections. Therefore, although bearing the limit of an underestimation, the final number is representative of the biological condition actually evaluated. When the number of analyzed sections is elevated and results derived from different experimental (normal vs diseased) groups are compared, data obtained by direct count at light microscopy might be more adherent to disease-induced biological changes. Nonetheless, we agree that on a theoretical basis $N = d/ns \sum x$ should express correctly neuron number according to a normal harmonic distribution of neuronal size and density within various areas of a given nucleus.

As a final consideration, it is worth highlighting the seminal role of the researcher in all phases of the stereology-like procedure. In fact, the expertise of the observer, consisting of specific technical and interpretative skills, represents a unique "tool", which is determinant for the correct execution of the entire protocol, even when unexpected deviation from the "normal" morphology and/or

topography occurs. This is the case of MN heterotopy found in SMA mice, which might be neglected in the absence of a direct observer who identifies hectopical MNs within the white matter of the spinal cord (Fulceri et al., 2012).

6. The count of motor neuron cell bodies does not account for motor neuron integrity

As a final critical issue, it is worth considering whether in MN disorders the amount of MN cell bodies is a reliable parameter for MN integrity. In a recent paper, it was demonstrated that in a mouse model of ALS, preservation of MN cell body by preserving mitochondrial integrity does not produce any positive effects on disease progression (Parone et al., 2013). This apparent discrepancy can be explained by considering that even when MN perikaria within the spinal cord are spared, axonal degeneration still persists at peripheral muscles (Natale et al., 2015). In fact, when analysis of MN integrity is extended to include peripheral axons, the amount of damage found in distal axons exceeds the damage within proximal axons, cell bodies and dendrites (Natale et al., 2015). Therefore, the new disease concept emerging from these findings poses the distal axonal compartment as key to establish the occurrence of MN degeneration at a very early asymptomatic stage, when MN cell body is still unaffected.

7. Concluding remarks

Here we described a stereology-like procedure for counting MNs based on: i) corrected identification of the region of interest; ii) analysis of the whole region of interest following an appropriate sampling procedure; iii) establishing size, site and histochemical criteria to identify MNs. This procedure represents an attempt to extend unbiased stereology. As unbiased stereology, the stereology-like procedure establishes a series of criteria, which take into account morphology, size and placement of MNs, and it also uses sampling procedures to minimize bias and rule out the chance of double counting MNs. Moreover, as a classic cell count, this procedure uses H&E-stained sections, emphasizing the role of the researcher in identifying MNs.

Remarkably, the very same procedure is suitable for different experimental conditions and purposes. For instance, in a paper published by our research group, the stereology-like procedure was adapted to count neural progenitor cells within the Lamina X of the lumbar spinal cord (Fornai et al., 2014). Finally, although the protocol considers counting MNs stained with H&E, this does not rule out the possibility to perform stereology-like MN count following immunohistochemistry and apply the very same size, site and morphological criteria used in H&E-stained MNs even to identify immune-stained MNs.

References

Abercrombie M. (1946). Estimation of nuclear population from microtome sections. Anat. Rec. 94, 239-247.

Ashrafi S., Lalancette-Hébert M., Friese A., Sigrist M., Arber S., Shneider N.A. and Kaltschmidt J.A. (2012). Wnt7A identifies embryonic γ-motor neurons and reveals early postnatal dependence of γ-motor neurons on a muscle spindle-derived signal. J. Neurosci. 32, 8725-8731.

Avossa D., Grandolfo M., Mazzarol F., Zatta M. and Ballerini L. (2006). Early signs of motoneuron vulnerability in a disease model system: characterization of transverse slice cultures of spinal cord isolated from embryonic ALS mice. Neuroscience 138, 1179-1194.

Azzouz M., Hottinger A., Paterna J.C., Zurn A.D. Aebischer P. and Büeler H. (2000). Increased motoneuron survival and improved neuromuscular function in transgenic ALS mice after intraspinal injection of an adeno-associated virus encoding Bcl-2. Hum. Mol. Genet. 9, 803-811.

Barazzoni A.M., Clavenzani P., Chiocchetti R., Bompadre G.A., Grandis A., Petrosino G., Costerbosa G.L. and Bortolami R. (2005). Localisation of recurrent laryngeal nerve motoneurons in the sheep by means of retrograde fluorescent labelling. Res. Vet. Sci. 78, 249-253.

Barber R.P., Phelps P.E. and Vaughn J.E. (1991). Generation patterns of immunocytochemically identified cholinergic neurons at autonomic levels of the rat spinal cord. J. Comp. Neurol. 311, 509-519.

Barbizan R. and Oliveira A.L. (2010). Impact of acute inflammation on spinal motoneuron synaptic plasticity following ventral root avulsion. J. Neuroinflammation 7, 29.

Battaglia G., Riozzi B., Bucci D., Di Menna L., Molinaro G., Pallottino S., Nicoletti F. and Bruno V. (2015). Activation of mGlu3 metabotropic glutamate receptors enhances GDNF and GLT-1 formation in the spinal cord and rescues motor neurons in the SOD-1 mouse model of amyotrophic lateral sclerosis. Neurobiol. Dis. 74,126-136.

Benes F.M. and Lange N. (2001). Two-dimensional versus three-dimensional cell counting: a practical perspective. Trends Neurosci. 24, 11-17.

Berglund A.M. and Ryugo D.K. (1991). Neurofilament antibodies and spiral ganglion neurons of the mammalian cochlea. J. Comp. Neurol. 306, 393-408.

Biagioni F., Ferrucci M., Ryskalin L., Fulceri F., Lazzeri G., Calierno M.T., Busceti C.L., Ruffoli R. and Fornai F. (2017). Protective effects of long-term lithium administration in a slowly progressive SMA mouse model. Arch. Ital. Biol., in press.

Blizzard C.A., Lee K.M. and Dickson T.C. (2016). Inducing Chronic Excitotoxicity in the Mouse Spinal Cord to Investigate Lower Motor Neuron Degeneration. Front. Neurosci. 10, 76.

Braendgaard H. and Gundersen H.J.G. (1986). The impact of recent stereological advances on quantitative studies of the nervous system. J. Neurosci. Methods 18, 39-78.

Brown A.G. and Fyffe R.E. (1981). Direct observations on the contacts made between Ia afferent fibres and alpha-motoneurones in the cat's lumbosacral spinal cord. J. Physiol. 313, 121-140.

Bryan I.A., Trevino D.L. and Willis W.D. (1972). Evidence for a common location of alpha and gamma motoneurons. Brain Res. 38, 193-196.

Bucher S., Braunstein K.E., Niessen H.G. Kaulisch T., Neumaier M., Boeckers T.M., Stiller D. and Ludolph A.C. (2007). Vacuolization correlates with spin-spin relaxation time in motor brainstem nuclei and behavioural tests in the transgenic G93A-SOD1 mouse model of ALS. Eur. J. Neurosci. 26, 1895-1901.

Burke R., Lundberg A. and Weight F. (1971). Spinal Border Cell Origin of the Ventral Spinocerebellar Tract. Exp. Brain Res. 12, 283-294.

Buttry J.L. and Goshgarian H.G. (2015). WGA-Alexa transsynaptic labeling in the phrenic motor system of adult rats: Intrapleural injection versus intradiaphragmatic injection. J. Neurosci. Methods 241, 137–145.

Campbell M.J. and Morrison J. (1989). Monoclonal antibody to neurofilament protein (SMI 32) labels a subpopulation of pyramidal neurons in the human and monkey neocortex. J. Comp. Neurol. 282, 191–205.

Carriedo S.G., Yin H.Z., Lamberta R. and Weiss J.H. (1995). In vitro kainate injury to large SMI-32(+) spinal neurons is Ca2+ dependent. Neuroreport 6, 945–948.

Carriedo S.G., Yin H.Z. and Weiss J. H. (1996). Motor neurons are selectively vulnerable to AMPA/Kainate receptor-mediated injury in vitro. J. Neurosci. 16, 4069–4079.

Casas C., Herrando-Grabulosa M., Manzano R., Mancuso R., Osta R. and Navarro X. (2013). Early presymptomatic cholinergic dysfunction in a murine model of amyotrophic lateral sclerosis. Brain Behav. 3, 145-158.

Cauchi R.J. (2014). Gem depletion: amyotrophic lateral sclerosis and spinal muscular atrophy crossover. CNS Neurosci. Ther. 20, 574–581.

Chang Q. and Martin L.J. (2011). Glycine receptor channels in spinal motoneurons are abnormal in a transgenic mouse model of amyotrophic lateral sclerosis. J. Neurosci. 31, 2815-2827.

Chi L., Ke Y., Luo C., Li B., Gozal D., Kalyanaraman B. and Liu R. (2006). Motor neuron degeneration promotes neural progenitor cell proliferation, migration, and neurogenesis in the spinal cords of amyotrophic lateral sclerosis mice. Stem Cells 24, 34-43.

Chopek J.W. and Gardiner P.F. (2010). Life-long caloric restriction: Effect on age-related changes in motoneuron numbers, sizes and apoptotic markers. Mech. Ageing Dev. 131, 650-659.

Chou S.M. and Wang H.S. (1997). Aberrant glycosylation/phoshorylation in chromatolytic motoneurons of Werdnig–Hoffmann disease. J. Neurol. Sci. 152, 198-209.

Ciavarro G.L., Calvaresi N., Botturi A., Bendotti C., Andreoni G. and Pedotti A. (2003). The densitometric physical fractionator for counting neuronal populations: application to a mouse model of familial amyotrophic lateral sclerosis. J. Neurosci. Methods. 129, 61-71.

Clarac F. and Barbara J.G. (2011). The emergence of the "motoneuron concept": from the early 19th C to the beginning of the 20th C. Brain Res. 1409, 23-41.

Cooper S. and Sherrington C.S. (1940). Gower's tract and the spinal border cells. Brain. 63, 123-134.

Cruz-Orive, L.M. (1997). Stereology of single objects. J. Microsc. 186, 93-107.

Cruz-Orive L.M. (2004). Precision of the fractionators from cavalieri designs. J. Microsc. 213, 205-211.

Cruz-Sánchez F.F., Moral A., Tolosa E., de Belleroche J. and Rossi M.L. (1998). Evaluation of neuronal loss, astrocytosis and abnormalities of cytoskeletal components of large motor neurons in the human anterior horn in aging. J. Neural. Transm. 105, 689-701.

D'Errico P., Boido M., Piras A., Valsecchi V., De Amicis E., Locatelli D., Capra S., Vagni F., Vercelli A. and Battaglia G. (2013). Selective vulnerability of spinal and cortical motor neuron subpopulations in delta7 SMA mice. PLoS One. 8:e82654.

Dachs E., Hereu M., Piedrafita L., Casanovas A., Calderó J. and Esquerda J.E. (2011). Defective neuromuscular junction organization and postnatal myogenesis in mice with severe spinal muscular atrophy. J. Neuropathol. Exp. Neurol. 70: 444-461.

Dachs E., Piedrafita L., Hereu M., Esquerda J.E. and Calderó J. (2013). Chronic treatment with lithium does not improve neuromuscular phenotype in a mouse model of severe spinal muscular atrophy. Neuroscience 250, 417-433.

Dal Canto M.C. and Gurney M.E. (1997). A low expressor line of transgenic mice carrying a mutant human Cu,Zn superoxide dismutase (SOD1) gene develops pathological changes that most closely resemble those in human amyotrophic lateral sclerosis. Acta Neuropathol. 93, 537-550.

Dudek A., Sienkiewicz W., Marczak M. and Kaleczyc J. (2011). Immunohistochemical properties of motoneurons supplying the trapezius muscle in the rat. Pol. J. Vet. Sci. 14, 199–205.

Dziedzic T., Metz I., Dallenga T., König F. B., Müller S., Stadelmann C. and Brück W. (2010). Wallerian degeneration: a major component of early axonal pathology in multiple sclerosis. Brain Pathol. 20, 976–985.

Dziewulska D., Gogol A., Gogol P. and Rafalowska J. (2013). Enlargement of the Nissl substance as a manifestation of early damage to spinal cord motoneurons in amyotrophic lateral sclerosis. Clin. Neuropathol. 32, 480-485.

Eccles J.C., Fatt P. and Koketsu K. (1954). Cholinergic and inhibitory synapses in a pathway from motor axon collaterals to motoneurones. J. Physiol. 126, 524-562.

Eccles J.C., Eccles R.M., Iggo A. and Lundberg A. (1960). Electrophysiological studies on gamma motor neurones. Acta Physiol. Scand. 50, 32-40.

Edwards I.J., Bruce G., Lawrenson C., Howe L., Clapcote S.J., Deuchars S.A. and Deuchars J. (2013). Na+/K+ ATPase alpha1 and alpha3 isoforms are differentially expressed in alpha- and gamma-motoneurons. J. Neurosci. 33, 9913-9919.

Elliott H.C. (1942). Studies on the motor cells of the spinal cord. I Distribution in the normal human cord. Am. J. Anat. 70, 95-117.

Elliott H.C. (1944). Studies on the motor cells of the spinal cord. IV. Distribution in experimental animals. J. Comp. Neurol. 81, 97-103.

Enjin A., Leão K.E., Mikulovic S., Le Merre P., Tourtellotte W.G. and Kullander K. (2012). Sensorimotor function is modulated by the serotonin receptor 1d, a novel marker for gamma motor neurons. Mol. Cell. Neurosci. 49, 322-332.

Evans M.C., Modo M., Talbot K., Sibson N. and Turner M.R. (2012). Magnetic resonance imaging of pathological processes in rodent models of amyotrophic lateral sclerosis. Amyotroph. Lateral Scler. 13, 288-301.

Faunes M., Oñate-Ponce A., Fernández-Collemann S. and Henny P. (2016). Excitatory and inhibitory innervation of the mouse orofacial motor nuclei: A stereological study. J. Comp. Neurol. 524, 738-758.

Fayzullina S. and Martin L.J. (2014). Skeletal muscle DNA damage precedes spinal motor neuron DNA damage in a mouse model of Spinal Muscular Atrophy (SMA). PLoS One 9:e93329.

Ferrucci M., Spalloni A., Bartalucci A., Cantafora E., Fulceri F., Nutini M., Longone P., Paparelli A. and Fornai F. (2010). A systematic study of brainstem motor nuclei in a mouse model of ALS, the effects of lithium. Neurobiol. Dis. 37, 370-383.

Fornai F., Longone P., Cafaro L., Kastsiuchenka O., Ferrucci M., Manca M.L., Lazzeri G., Spalloni A., Bellio N., Lenzi P., Modugno N., Siciliano G., Isidoro C., Murri L., Ruggieri S. and Paparelli A. (2008a). Lithium delays progression of amyotrophic lateral sclerosis. Proc. Natl. Acad. Sci. U S A. 105, 2052-2057. Erratum in: (2008) Proc. Natl. Acad. Sci. U S A. 105, 16404-16407.

Fornai F., Longone P., Ferrucci M., Lenzi P., Isidoro C., Ruggieri S. and Paparelli A. (2008b). Autophagy and amyotrophic lateral sclerosis: The multiple roles of lithium. Autophagy 4: 527-530.

Fornai F., Ferrucci M., Lenzi P., Falleni A., Biagioni F., Flaibani M., Siciliano G., Giannessi F. and Paparelli A. (2014). Plastic changes in the spinal cord in motor neuron disease. Biomed. Res. Int. 670756.

Friese A., Kaltschmidt J.A., Ladle D.R., Sigrist M., Jessell T.M. and Arber S. (2009). Gamma and alpha motor neurons distinguished by expression of transcription factor Err3. Proc. Natl. Acad. Sci. USA 106, 13588-13593.

Fu Y., Sengul G., Paxinos G. and Watson C. (2012). The spinal precerebellar nuclei: calcium binding proteins and gene expression profile in the mouse. Neurosci. Lett. 518, 161-166.

Fu R., Tang Y., Ling Z.M., Li Y.Q., Cheng X., Song F.H., Zhou L.H. and Wu W. (2014). Lithium enhances survival and regrowth of spinal motoneurons after ventral root avulsion. BMC Neurosci. 2, 15-84.

Fulceri F., Bartalucci A., Paparelli S., Pasquali L., Biagioni F., Ferrucci M., Ruffoli R. and Fornai F. (2012). Motor neuron pathology and behavioral alterations at late stages in a SMA mouse model. Brain Res. 1442, 66-75.

Fulceri F., Ferrucci M., Lazzeri G., Paparelli S., Bartalucci A., Tamburini I., Paparelli A. and Fornai F. (2011). Autophagy activation in glutamate-induced motor neuron loss. Arch. Ital. Biol. 149, 101-111.

Gama-Carvalho M., L Garcia-Vaquero M., R Pinto F., Besse F., Weis J., Voigt A., Schulz J.B. and De Las Rivas J. (2017). Linking amyotrophic lateral sclerosis and spinal muscular atrophy through RNA-transcriptome homeostasis: a genomics perspective. J. Neurochem. 141, 12-30.

Goldstein M.E., Cooper H.S., Bruce J., Carde, M.J., Lee V.M. and Schlaepfer, W.W. (1987). Phosphorylation of neurofilament proteins and chromatolysis following transection of rat sciatic nerve. J. Neurosci. 7, 1586-1594.

Golub V.M., Brewer J., Wu X., Kuruba R., Short J., Manchi M., Swonke M., Younus I. and Reddy D.S. (2015). Neurostereology protocol for unbiased quantification of neuronal injury and neurodegeneration. Front. Aging Neurosci. 7, 196.

Gotts J., Atkinson L., Yanagawa Y., Deuchars J. and Deuchars, S.A. (2016). Co-expression of GAD67 and choline acetyltransferase in neurons in the mouse spinal cord: A focus on lamina X. Brain Res. 1646, 570-579.

Gundersen H.J. (1986). Stereology of arbitrary particles. A review of unbiased number and size estimators and the presentation of some new ones, in memory of William R. Thompson. J. Microsc. 143, 3-45.

Gundersen H.J.G. and Jensen E.B. (1987). The efficiency of systematic sampling in stereology and its prediction J. Microsc. 147, 229-263.

Ha H. and Liu C.N. (1968). Cell origin of the ventral spinocerebellar tract. J. Comp. Neurol. 133, 185-206.

Haenggeli C. and Kato A.C. (2002a). Rapid and reproducible methods using fluorogold for labelling a subpopulation of cervical motoneurons: application in the wobbler mouse. J. Neurosci. Methods. 116, 119-124.

Haenggeli C. and Kato A.C. (2002b). Differential vulnerability of cranial motoneurons in mouse models with motor neuron degeneration. Neurosci. Lett. 33, 39-43.

Hancock M.B. and Peveto, C.A. (1979). A preganglionic autonomic nucleus in the dorsal gray commissure of the lumbar spinal cord of the rat. J. Comp. Neurol. 183, 65-72.

Harding D.I., Greensmith L. and Vrbová G. (1999). Stabilizing neuromuscular contacts reduces motoneuron death caused by paralysis of muscles in neonatal rats. Neuroscience 93, 1141-1146.

Harrington E.P., Zhao C., Fancy S.P., Kaing S., Franklin R.J. and Rowitch D.H. (2010). Oligodendrocyte PTEN is required for myelin and axonal integrity, not remyelination. Ann. Neurol. 68, 703-716.

Hashizume K and Kanda K. (1995). Differential effects of aging on motoneurons andperipheral nerves innervating the hindlimb and forelimb muscles of rats. Neurosci. Res. 22, 189-196.

Hashizume K., Kanda K. and Burke R.E. (1988). Medial gastrocnemius motor nucleus in the rat: age-related changes in the number and size of motoneurons. J. Comp. Neurol. 269, 425-430.

Hayashi A., Moradzadeh A., Hunter D.A., Kawamura D.H., Puppala V.K., Tung T.H., Mackinnon S.E. and Myckatyn T.M. (2007). Retrograde labeling in peripheral nerve research: it is not all black and white. J. Reconstr. Microsurg. 23, 381-389.

He B.P.,and Strong,M.J. (2000). A morphological analysis of the motor neuron degeneration and microglial reaction in acute and chronic in vivo aluminum chloride neurotoxicity. J. Chem. Neuroanat. 17, 207-215.

Hervias I., Beal M.F. and Manfredi G. (2006). Mitochondrial dysfunction and amyotrophic lateral sclerosis. Muscle Nerve. 33, 598-608.

Hopkins D.A. and Armour J.A. (1998). Brainstem cells of origin of physiologically identified cardiopulmonary nerves in the rhesus monkey (Macaca mulatta). J. Auton. Nerv. Syst. 68, 21-32.

Hubbard J.I. and Oscarsson O. (1961). Localization of the cells of origin of the ventral spino-cerebellar tract. Nature 189, 157-158.

Huisinga K.L., Brower-Toland B. and Elgin S.C.R. (2006). The contradictory definitions of heterochromatin: Transcription and silencing. Chromosoma 115, 110-122.

Irving D., Rebeiz, J.J. and Tomlinson B.E. (1974). Numbers of limb motor neurones in the individual segments of the human lumbosacral spinal cord. J. Neurol. Sci. 21, 203-212.

Ishida H., Inoue K.I., Takada M. and Hoshi E. (2015). Origins of multisynaptic projections from the basal ganglia to the forelimb region of the ventral premotor cortex in macaque monkeys. Eur. J. Neurosci. 21, 203-212.

Ishihara A. and Araki H. (1988). Effects of age on the number and histochemical properties of muscle fibers and motoneurons in the rat extensor digitorum longus muscle. Mech. Ageing Dev. 45, 213-221.

Jara J.H., Genç B., Klessner J.L. and Ozdinler P.H. (2014). Retrograde labeling, transduction, and genetic targeting allow cellular analysis of corticospinal motor neurons: implications in health and disease. Front. Neuroanat. 8, 16.

Johnson I.P. (1986). A quantitative ultrastructural comparison of alpha and gamma motoneurons in the thoracic region of the spinal cord of the adult cat. J. Anat. 147, 55-72.

Karalija A., Novikova L.N., Kingham P.J., Wiberg M. and Novikov L.N. (2012). Neuroprotective effects of N-acetyl-cysteine and acetyl-L-carnitine after spinal cord injury in adult rats. PLoS One 7, e41086.

Kasumacic N., Lambert F.M., Coulon P., Bras H., Vinay L., Perreault M.C., Glover J.C. (2015). Segmental organization of vestibulospinal inputs to spinal interneurons mediating crossed activation of thoracolumbar motoneurons in the neonatal mouse. J. Neurosci. 35, 8158–8169.

Kawamura Y., O'Brien P., Okazaki H. and Dyck P.J. (1977). Lumbar motoneurons of man II: the number and diameter distribution of large- and intermediate-diameter cytons in "motoneuron columns" of spinal cord of man. J. Neuropathol. Exp. Neurol. 36, 861-870.

Kim J.H. and Song S.K. (2013). Diffusion tensor imaging of the mouse brainstem and cervical spinal cord. Nat. Protoc. 8, 409-417.

King M.A., Scotty N., Klein R.L. and Meyer E.M. (2002). Particle detection, number estimation, and feature measurement in gene transfer studies: optical fractionator stereology integrated with digital image processing and analysis. Methods 28, 293-299.

Konigsmark B.W. (1970). Methods for the counting of neurons, in Contemporary Research Methods in Neuroanatomy. W.J.H. Nauta and S.O.E. Ebbesson (eds). Springer-Verlag. New York. pp 315-338.

Kretschmann H.J., Tafesse U. and Herrmann A. (1982). Different volume changes of cerebral cortex and white matter during histological preparation. Mikrosk. Acta 86,13-24.

Kristensson K.,and Olsson,Y. (1971). Retrograde axonal transport of protein. Brain Res. 29, 363-365.

Lalancette-Hebert M., Sharma A., Lyashchenko A.K. and Shneider N.A. (2016). Gamma motor neurons survive and exacerbate alpha motor neuron degeneration in ALS. Proc. Natl. Acad. Sci. USA 113, E8316-E8325.

LaVail J.H. and LaVai, M.M. (1972). Retrograde axonal transport in the central nervous system. Science. 176, 1416.

Lever T.E., Gorsek A., Cox K.T., O'Brien K.F., Capra N.F., Hough M.S. and Murashov A.K. (2009). An animal model of oral dysphagia in amyotrophic lateral sclerosis. Dysphagia 24, 180-195.

Li S.Y., Chen Y.L., Zeng J.Y., Xie W.Q. and Kang Z. M. (2015) Melanocortin-4 receptor expression in autonomic circuitry involved in gastric function. Int. J. Clin. Exp. Med. 8, 4152-4157.

Lieberman A.R. (1971). The axon reaction: a review of the principal features of perikaryal responses to axon injury. Int. Rev. Neurobiol. 14, 49-124.

Lladó J., Haenggeli C., Pardo A., Wong V., Benson L., Coccia C., Rothstein J.D., Shefner J.M. and Maragakis N.J. (2006). Degeneration of respiratory motor neurons in the SOD1 G93A transgenic rat model of ALS. Neurobiol. Dis. 21, 110-118.

Maeda M., Harris A.W., Kingha, B.F., Lumpkin C.J., Opdenaker L.M., McCahan S.M., Wang W. and Butchbach M.E. (2014). Transcriptome profiling of spinal muscular atrophy motor neurons derived from mouse embryonic stem cells. PLoS One. 9, e106818.

Mantilla C.B., Zhan W.Z. and Sieck G.C. (2009). Retrograde labeling of phrenic motoneurons by intrapleural injection. J. Neurosci. Methods 182, 244-249.

Martin, L.J., Liu Z., Chen K., Price A.C., Pan Y., Swaby J.A. and Golden W.C. (2007). Motor Neuron Degeneration in Amyotrophic Lateral Sclerosis Mutant Superoxide Dismutase-1 Transgenic Mice: Mechanisms of Mitochondriopathy and Cell Death. J. Comp. Neurol. 500, 20-46.

Martinez T.L., Kong L., Wang X., Osborne M.A., Crowder M.E., Van Meerbeke J.P., Xu X., Davis C., Wooley J., Goldhamer D.J., Lutz C.M., Rich M.M. and Sumner C.J. (2012). SMN in motor neurons determines synaptic integrity in spinal muscular atrophy. J. Neurosci. 32, 8703-8715.

Matsumoto A. (1998). Synaptic changes in the perineal motoneurons of aged male rats. J. Comp. Neurol. 400, 103-109.

Mayhew T.M. (2014). Quantitative immunocytochemistry at the ultrastructural level: a stereology-based approach to molecular nanomorphomics. Cell Tissue Res. 11, 43-59.

McBride D.K. and Schmorrow D. (2005). Quantifying Human Information Processing. Lexington Books, Rowman and Littlefield Publishers, Inc. Lanham, MD (USA). pp. 270.

Menzies F.M., Ince P.G. and Shaw P.J. (2002). Mitochondrial involvement in amyotrophic lateral sclerosis. Neurochem. Int. 40, 543-551.

Mesulam M.M. (1978). Tetramethyl benzidine for horseradish peroxidase neuroistochemistry: a non-carcinogenic blue reaction product with superior sensitivity for visualizing neural afferents and efferents. J. Histochem. Cytochem. 26, 106-117.

Mesulam M. and Geula C. (1991). Differential distribution of a neurofilament protein epitope in acetylcholinesterase-rich neurons of human cerebral neocortex. Brain Res. 544, 169-173.

Miles G.B. Hartle, R., Todd A.J. and Brownstone R.M. (2007). Spinal cholinergic interneurons regulate the excitability of motoneurons during locomotion. Proc. Natl. Acad. Sci. USA 104, 2448-2453.

Monani U.R., Sendtner M., Coovert D.D., Parsons D.W., Andreassi C., Le T.T., Jablonka S., Schrank B., Rossoll W., Prior T.W., Morris G.E. and Burghes A.H. (2000). The human centromeric survival motor neuron gene (SMN2) rescues embryonic lethality in Smn(-/-) mice and results in a mouse with spinal muscular atrophy. Hum. Mol. Genet. 9, 333-339. Erratum in. (2007) Hum. Mol. Genet. 16: 2648.

Morel A., Loup F., Magnin M. and Jeanmonod D. (2002). Neurochemical organization of the human basal ganglia: anatomofunctional territories defined by the distributions of calcium-binding proteins and SMI-32. J. Comp. Neurol. 443, 86-103.

Morrison B.M., Janssen W.G., Gordon J.W. and Morrison J.H. (1998). Time course of neuropathology in the spinal cord of G86R superoxide dismutase transgenic mice. J. Comp. Neurol. 391, 64-77.

Nagao M., Misawa H., Kato S. and Hirai S. (1998). Loss of cholinergic synapses on the spinal motor neurons of amyotrophic lateral sclerosis. J. Neuropathol. Exp. Neurol. 57, 329-333.

Natale G., Lenzi P., Lazzeri G., Falleni A., Biagioni F., Ryskalin L. and Fornai F. (2015). Compartment-dependent mitochondrial alterations in experimental ALS, the effects of mitophagy and mitochondriogenesis. Front. Cell Neurosci. 9, 434.

Niessen H.G., Angenstein F., Sander K., Kunz W.S., Teuchert M., Ludolph A.C., Heinze H.J., Scheich H. and Vielhaber S. (2006). In vivo quantification of spinal and bulbar motor neuron degeneration in the G93A-SOD1 transgenic mouse model of ALS by T2 relaxation time and apparent diffusion coefficient. Exp. Neurol. 201, 293-300.

Nijssen J., Comley L.H. and Hedlund E. (2017). Motor neuron vulnerability and resistance in amyotrophic lateral sclerosis. Acta Neuropathol. 133, 863-885.

Nimchinsky E.A., Young W.G., Yeung G., Shah R.A., Gordon J.W., Bloom F.E., Morrison J.H. and Hof P.R. (2000). Differential vulnerability of oculomotor, facial, and hypoglossal nuclei in G86R superoxide dismutase transgenic mice. J. Comp. Neurol. 416, 112-125.

Oda Y., Imai S., Nakanishi I., Ichikawa T. and Deguchi T. (1995). Immunohistochemical study on choline acetyltransferase in the spinal cord of patients with amyotrophic lateral sclerosis. Pathol. Int. 45, 933-939.

Ogata J. and Feigin I. (1973). The relative weight of the gray and white matter of the normal human brain. J. Neuropathol. Exp. Neurol. 32, 585-588.

Oppenheim R.W. and Heaton M.B. (1975). The retrograde transport of horseradish peroxidase from the developing limb of the chick embryo. Brain Res. 98, 291-302.

Palomo G.M. and Manfredi G. (2015). Exploring new pathways of neurodegeneration in ALS: the role of mitochondria quality control. Brain Res. 1607, 36-46.

Papapetropoulos T.A. and Bradley W.G. (1972). Spinal motor neurones in murine muscular dystrophy and spinal muscular atrophy. A quantitative histological study. J. Neurol. Neurosurg. Psychiatry 35, 60-65.

Parone P.A., Da Cruz S., Han J.S., McAlonis-Downes M., Vetto A.P., Lee S.K., Tseng E. and Cleveland D.W. (2013). Enhancing mitochondrial calcium buffering capacity reduces aggregation of misfolded SOD1 and motor neuron cell death without extending survival in mouse models of inherited amyotrophic lateral sclerosis. J. Neurosci. 33, 4657-4671.

Pasquali L., Longone P., Isidoro C., Ruggieri S., Paparelli A. and Fornai F. (2009). Autophagy, lithium, and amyotrophic lateral sclerosis. Muscle Nerve 40, 173-194.

Paxinos G. and Franklin K.B.J. (2004). The mouse brain in stereotaxic coordinates. 2nd Edition. Academic Press. San Diego, USA.

Penet M.F., Laigle C., Fur Y.L., Confort-Gouny S., Heurteaux C., Cozzone P.J. and Viola A. (2006). In vivo characterization of brain morphometric and metabolic endophenotypes in three inbred strains of mice using magnetic resonance techniques. Behav. Genet. 36, 732-744.

Pereira M.A., Dias A.R., Faraj S.F., Cirqueira C. dos S., Tomitao M.T., Nahas S.C., Ribeiro U. Jr. and de Mello E.S. (2015). Carnoy's solution is an adequate tissue fixative for routine surgical pathology, preserving cell morphology and molecular integrity. Histopathology 66, 388-397.

Phelps P.E., Barber R.P., Brennan L.A., Maines V.M., Salvaterra P.M. and Vaughn J.E. (1990). Embryonic development of four different subsets of cholinergic neurons in rat cervical spinal cord. J. Comp. Neurol. 291, 9-26.

Powis R.A. and Gillingwater T.H. (2016). Selective loss of alpha motor neurons with sparing of gamma motor neurons and spinal cord cholinergic neurons in a mouse model of spinal muscular atrophy. J. Anat. 228, 443-451.

Pun S., Santos A.F., Saxena S., Xu L. and Caroni P. (2006). Selective vulnerability and pruning of phasic motoneuron axons in motoneuron disease alleviated by CNTF. Nat. Neurosci. 9, 408-419.

Quester R. and Schröder R. (1997). The shrinkage of the human brain stem during formalin fixation and embedding in paraffin. J. Neurosci. Methods 75, 81-89.

Ramanathan S., Combes D., Molinari M., Simmers J. and Sillar K.T. (2006). Developmental and regional expression of NADPH-diaphorase/nitric oxide synthase in spinal cord neurons correlates with the emergence of limb motor networks in metamorphosing Xenopus laevis. Eur. J. Neurosci. 24, 1907–1922.

Ramírez-Jarquín U.N., Lazo-Gómez R., Tovar-Y-Romo L.B. and Tapia R. (2014). Spinal inhibitory circuits and their role in motor neuron degeneration. Neuropharmacol. 82, 101-117.

Ramón y Cajal S. (1889). Coloración por el método de Golgi de los centros nervoso de los embriones de pollo y Nuevas aplicaciones del método de coloración de Golgi. La Gaceta Médica Catalana, n1.

Ramón y Cajal S. (1909). Histologie du Système Nerveux de l'Homme et des Vertébrés (Histology of the Nervous System of Man and Vertebrates). Maloine (ed). Paris.

Ramón y Cajal S. (1911). Histologie du Système Nerveux de l'Homme et des Vertébrés [Histology of the Nervous System of Man and Vertebrates. 2nd Edition Maloine (ed). Paris. Instituto Ramón y Cajal. Raycar, SA, Madrid, 1972.

Ravits J., Laurie P., Fan Y. and Moore D.H. (2007). Implications of ALS focality. Neurology. 68, 1576-1581.

Rende M., Hagg T., Manthorpe M. and Varon S. (1992). Nerve growth factor receptor immunoreactivity in neurons of the normal adult rat spinal cord and its modulation after peripheral nerve lesions. J. Comp. Neurol. 319, 285-298.

Rende M., Provenzano C. and Tonali P. (1993). Modulation of low-affinity nerve growth factor receptor in injured adult rat spinal cord motoneurons. J. Comp. Neurol. 338, 560-574.

Rende M., Giambanco I., Buratta M. and Tonali P. (1995). Axotomy induces a different modulation of both low-affinity nerve growth factor receptor and choline acetyltransferase between adult rat spinal and brainstem motoneurons. J. Comp. Neurol. 363, 249-263.

Rexed B. (1952). The cytoarchitectonic organization of the spinal cord in the cat. J. Comp. Neurol. 96, 414-495.

Rexed B. (1954). A cytoarchitectonic atlas of the spinal cord in the cat. J. Comp. Neurol. 100, 297-379.

Rice C.D., Weber S.A., Waggoner A.L., Jessell M.E. and Yates B.J. (2010). Mapping of neural pathways that influence diaphragm activity and project to the lumbar spinal cord in cats. Exp. Brain Res. 203, 205–211.

Richmond F.J., Gladdy R., Creasy J.L., Kitamura S., Smits E. and Thomson D.B. (1994). Efficacy of seven retrograde tracers, compared in multiple-labelling studies of feline motoneurons. J. Neurosci. Methods. 53, 35-46. Erratum in: (1995) J. Neurosci. Methods 58, 221.

Rodriguez-Muela N., Litterman N.K., Norabuena E.M, Mull J.L., Galazo M.J., Sun C., Ng S.Y., Makhortova N.R., White A., Lynes M.M., Chung W.K., Davidow L.S., Macklis J.D. and Rubin L.L. (2017). Single-Cell Analysis of SMN Reveals Its Broader Role in Neuromuscular Disease. Cell Rep. 18, 1484-1498.

Romanes G.J. (1951). The motor cell columns in the lumbosacral spinal cord of the cat. J. Comp. Neurol. 94, 313-364.

Romanes G.J. (1964). The motor pools of the spinal cord. Prog. Brain Res. 11, 93-119.

Ruffoli R., Bartalucci A., Frati A. and Fornai F. (2015). Ultrastructural studies of ALS mitochondria connect altered function and permeability with defects of mitophagy and mitochondriogenesis. Front. Cell. Neurosci. 9, 341.

Ruffoli R., Biagioni F., Busceti C.L., Gaglione A., Ryskalin L., Gambardella S., Frati A. and Fornai F. (2017). Neurons other than motor neurons in motor neuron disease. Histol. Histopathol. Apr 11:11895. doi: 10.14670/HH-11-895. [Epub ahead of print].

Sauer H. and Oertel W.H. (1994). Progressive degeneration of nigrostriatal dopamine neurons following intrastriatal terminal lesions with 6-hydroxydopamine: A combined retrograde tracing and immunocytochemical study in the rat. Neuroscience. 59, 401-415.

Saxena K., Patro N. and Patro I. (2007). FK506 protects neurons following peripheral nerve injury via immunosuppression. Cell Mol. Neurobiol. 27, 1049-1057.

Schaffner A.E., St. John P.A. and Barker J.L. (1987). Fluorescence-activated cell sorting of embryonic mouse and rat motoneurons and their long-term survival *in vitro*. J. Neurosci. 7, 3088-3104.

Schmitz C. and Hof P.R. (2005). Design-based stereology in neuroscience. Neuroscience 130, 813-831.

Schmitz C. and Hof P.R. (2007). Design-based stereology in Brain Aging Research. In: Brain Aging: Models, Methods and Mechanisms. Riddle D.R. (ed). CRC Press. Boca Raton, FL (USA). pp 64-96.

Shneider N.A., Brown M.N., Smith C.A., Pickel J. and Alvarez F.J. (2009). Gamma motor neurons express distinct genetic markers at birth and require muscle spindle-derived GDNF for postnatal survival. Neural Dev. 4, 42.

Schwarz E.C., Thompson J.M., Connor N.P. and Behan M. (2009) The effects of aging on hypoglossal motoneurons in rats. Dysphagia 24, 40-48.

Siembab V.C., Gomez-Perez L., Rotterman T.M., Shneider N.A. and Alvarez F.J. (2016). Role of primary afferents in the developmental regulation of motor axon synapse numbers on Renshaw cells. J. Comp. Neurol. 524, 1892-1919.

Simic G., Mladinov M., Seso-Simic D., Jovanov-Milosevic N., Islam A., Pajtak A., Barisic N., Sertic J., Lucassen P.J., Hof P.R. and Kruslin B. (2008). Abnormal motoneuron migration, differentiation and axon outgrowth in spinal muscular atrophy. Acta Neuropathol. 115, 313-326.

Singh R.N., Howell M.D., Ottesen E.W. and Singh N.N. (2017). Diverse role of survival motor neuron protein. Biochim. Biophys. Acta. 1860, 299-315.

Singhal P., Singh N.N., Sreedhar G., Banerjee S., Batra M. and Garg A. (2016). Evaluation of Histomorphometric Changes in Tissue Architecture in Relation to Alteration inFixation Protocol - An Invitro Study. J. Clin. Diagn. Res. 10, ZC28-32.

Skup M., Gajewska-Wozniak O., Grygielewicz P., Mankovskaya T. and Czarkowska-Bauch J. (2012). Different effects of spinalization and locomotor training of spinal animals on cholinergic innervation of the soleus and tibialis anterior motoneurons. Eur. J. Neurosci. 36, 2679–2688.

Sohal G.S. and Holt R.K. (1978). Identification of the trochlear motoneurons by retrograde transport of horseradish peroxidase. Exp.Neurol. 59, 509-514.

Sprague J.M. (1953). Spinal "Border Cells" and their role in postural mechanism (Sehiff-Sherrington phenomenon). J. Neurophysiol. 16, 464-474.

Stephens B., Guiloff R.J., Navarrete R., Newman P., Nikhar N. and Lewis P. (2006). Widespread loss of neuronal populations in the spinal ventral horn in sporadic motor neuron disease. A morphometric study. J. Neurol. Sci. 244, 41-58.

Stepien A.E., Tripodi M. and Arber S. (2010). Monosynaptic rabies virus reveals premotor network organization and synaptic specificity of cholinergic partition cells. Neuron 68, 456-472.

Sterio D.C. (1984). The unbiased estimation of number and sizes of arbitrary particles using the disector. J. Microsc. 134, 127-136.

Straznicky C., Vickers J. C., Gábriel R. and Costa M. (1992). A neurofilament protein antibody selectively labels a large ganglion cell type in the human retina. Brain Res. 582, 123-128.

Suzuki M., McHugh J., Tork C., Shelley B., Klein S.M., Aebischer P. and Svendsen C.N. (2007). GDNF secreting human neural progenitor cells protect dying motor neurons, but not their projection to muscle, in a rat model of familial ALS. PLoS One. 2, e689.

Tandan R. and Bradley W.G. (1985). Amyotrophic lateral sclerosis: Part 1. Clinical features, pathology, and ethical issues in management. Ann. Neurol. 18, 271-280.

Thompson R.H. (2000). The Brain: A Neuroscience Primer. 3rd Edition. Worth Publishers. New York, NY (USA).

Tomlinson B.E., Irving D. and Rebeiz J.J. (1973). Total numbers of limb motor neurones in the human lumbosacral cord and an analysis of the accuracy of various sampling procedures. J. Neurol. Sci. 20, 313-327.

Tomlinson B.E., Walton J.N. and Irving D. (1974). Spinal cord limb motor neurones in muscular dystrophy. J. Neurol. Sci. 22, 305-327.

Tomlinson B.E. and Irving D. (1977). The numbers of limb motor neurones in the human lumbosacral cord throughout life. J. Neurol. Sci. 34, 213-219.

Truex R.C. and Carpenter M.B. (1969). Human neuroanatomy. 6th Edition. Williams and Wilkins. Baltimore, MD (USA).

Tsang Y.M., Chiong F., Kuznetsov D., Kasarskis E. and Geula C. (2000). Motor neurons are rich in non-phosphorylated neurofilaments: cross-species comparison and alterations in ALS. Brain Res. 861, 45–58.

Tsuiji H., Iguchi Y., Furuya A., Kataoka A., Hatsuta H., Atsuta N., Tanaka F., Hashizume Y., Akatsu H., Murayama S., Sobue G. and Yamanaka K. (2013). Spliceosome integrity is defective in the motor neuron diseases ALS and SMA. EMBO Mol. Med. 5, 221-234.

Ugolini G. (2011). Rabies virus as a transneuronal tracer of neuronal connections. Adv. Virus Res. 79, 165–202.

Von Kölliker A. (1854). Mikroskopische Anatomie oder Gewebelehre des Menschen (Human Microscopic Anatomy and Histology). Verlag von Wilhelm Engelman. Leipzig.

Von Kölliker A. and Turner W.A. (1891). The Minute Anatomy of the Spinal Cord and Cerebellum Demonstrated by Golgi's Method. J. Anat. Physiol. 25, 443-460.

Waerzeggers Y., Monfared P., Viel T., Winkeler, A. and Jacobs A.H. (2010). Mouse models in neurological disorders: applications of non-invasive imaging. Biochim. Biophys. Acta 1802, 819-839.

Wakayama I. (1992). Morphometry of spinal motor neurons in amyotrophic lateral sclerosis with special reference to chromatolysis and intracytoplasmic inclusion bodies. Brain Res. 586, 12-18.

Wang W., Nakadate K., Masugi-Tokita M., Shutoh F., Aziz W., Tarusawa E., Lorincz A., Molnár E., Kesaf S., Li Y.Q., Fukazawa Y., Nagao S. and Shigemoto R. (2014). Distinct cerebellar engrams in short-term and long-term motor learning. Proc. Natl. Acad. Sci. USA 111, E188-E193.

Watson C., Paxinos G., Kayaloglu G. and Heise C. (2009). Atlas of the Mouse Spinal Cord. In: The spinal cord. A Christopher and Dana Reeve Foundation Text and Atlas. Watson C., Paxinos G., Kayaloglu G. (eds). Academic Press. San Diego, CA (USA). pp. 308-379.

Webber S.C., Porter M.M. and Gardiner P.F. (2009). Modeling age-related neuromuscular changes in humans. Appl. Physiol. Nutr. Metab. 34, 732-744.

Weibel E.R. and Gomez D.M. (1962). A principle for counting tissue structures on random sections. J. Appl. Physiol. 17, 343-348.

West M.J., Slomianka L. and Gundersen H.J. (1991). Unbiased stereological estimation of the total number of neurons in the subdivisions of the rat hippocampus using the optical fractionator. Anat. Rec. 231, 482-497.

West M.J. (1999). Stereological methods for estimating the total number of neurons and synapses: issues of precision and bias. Trends Neurosci. 22, 51-61.

West M.J. (2002). Design-based stereological methods for counting neurons. Prog. Brain Res.135, 43.

West M.J. (2012a). Introduction to stereology. In: Basic Stereology for Biologists and Neuroscientists. Crotty D. (ed) Cold Spring Harbor Laboratory Press. NewYork, NY (USA). pp. 1-14.

West M.J. (2012b). Systematic versus random sampling in stereological studies. In: Basic Stereology for Biologists and Neuroscientists. Crotty D. (ed) Cold Spring Harbor Laboratory Press. NewYork, NY (USA). pp. 109-114.

Wetts R. and Vaughn J.E. (1996). Differential vulnerability of two subsets of spinal motor neurons in amyotrophic lateral sclerosis. Exp. Neurol. 141, 248-255.

White C.M., Greensmith L. and Vrbová G. (2000). Repeated stimuli for axonal growth causes motoneuron death in adult rats: the effect of botulinum toxin followed by partial denervation. Neuroscience 95, 1101–1109.

Williams C., Kozlowski M.A., Hinton D.R. and Miller C.A. (1990). Degeneration of spinocerebellar neurons in amyotrophic lateral sclerosis. Ann. Neurol. 27, 215-225.

Willis W.D., Skinner R.D. and Weir M.A. (1969). Field potentials of alpha and gamma motor neurones and Renshaw cells in response to activation of motor axons. Exp. Neurol. 25, 57-69.

Wiggins L.M., Kuta A., Stevens J.C., Fishe, E.M. and von Bartheld C.S. (2012). A novel phenotype for the dynein heavy chain mutation Loa: altered dendritic morphology, organelle density, and reduced numbers of trigeminal motoneurons. J. Comp. Neurol. 520, 2757-2773.

Xu H., Boychuk J.A., Boychuk C.R., Uteshev V.V. and Smith B.N. (2015). Nicotine enhances inhibition of mouse vagal motor neurons by modulating excitability of premotor GABAergic neurons in the nucleus tractus solitarii. J. Neurophysiol. 113, 1165–1174.

Yoo Y.E. and Ko C.P. (2012). Dihydrotestosterone ameliorates degeneration in muscle, axons and motoneurons and improves motor function in amyotrophic lateral sclerosis model mice. PLoS One. 7, e37258.

Yu Y.L., Li H.Y., Zhang P.X., Yin X.F., Han N., Kou Y.H. and Jiang B.G. (2015). Comparison of commonly used retrograde tracers in rat spinal motor neurons. Neural Regen. Res. 10, 1700-1705.

Zang D.W., Yang Q., Wang H.X., Egan G., Lopes E.C. and and Cheema S.S. (2004). Magnetic resonance imaging reveals neuronal degeneration in the brainstem of the superoxide dismutase 1 transgenic mouse model of amyotrophic lateral sclerosis. Eur. J. Neurosci. 20, 1745-1751.

Zhang C., Goto N., Suzuki M. and Ke M. (1996). Age-related reductions in number and size of anterior horn cells at C6 level of the human spinal cord. Okajimas Folia Anat. Jpn. 73, 171-177.

Figure legends

Figure 1. Histochemical visualization of motor neurons.

Histochemical stains currently used to visualize motor neurons include H&E, cresyl violet, and toluidine blue. **A**) Following H&E staining, motor neurons appear as intensely basophilic multipolar cells, lying within eosinophilic extracellular substance. Basophilic motor neurons are even more evident following **B**) cresyl violet or **C**) toluidine blue staining. In all these staining, large pale nuclei containing dark nucleoli, and cytoplasm filled with intensely basophilic material (namely, the "Nissl substance" of the past century) identify motor neurons.

Bar = 25 μm (**A**-**C**).

Figure 2. Immunohistochemistry fails to label specifically motor neurons

Representative immunohistochemistry anti- (**A**) SMI-32; (**B**) SMN; and (**C**) ChAT in the cervical spinal cord of mouse. As shown in each representative picture, despite labeling motor neurons none of these antibodies is specific for these cells. Pictures were counterstained with haematoxylin.

Bar = 220 μm (**A**-**C**).

Figure 3. Design-based stereology: optical disector probe in SMI-32 immune-stained lumbar spinal cord

(**A**) Anti-SMI-32 representative immunohistochemistry within lumbar spinal cord of a control mouse. This picture is used for design-based stereology, with optical disector, as shown in (**B**, **C**). The green line in (**B**) borders the area of interest (AOI, in this case the ventral horn of the mouse spinal cord, as decided by the operator). Disector frames measuring 40 μm x 40 μm (in red), drawn inside the AOI by the software Image Pro Plus 6.2 (in unbiased manner) represent the areas where, at higher magnification, the stereological count of motor neurons is actually carried out (**C**).

Bars = 500 μm (**A**, **B**); 10 μm (**C**).

Figure 4. SMI-32 immune-reactivity of motor neurons in ALS mice.

Motor neurons of control (**A**) and ALS (**B**) mice as evidenced by SMI-32 immunohistochemistry. The intensely homogeneous SMI-32 immune-reactivity of control motor neurons is lost in ALS motor neurons, due to the presence of large cytosolic vacuoles.

Bar = 10 μm.

Figure 5. Section thickness and image resolution.

H&E-stained spinal cord sections, cut at different thickness: (**A**) Representative 8 μm-thick slice showing neurons with intensely basophilic cytoplasm, and nucleoli, pale nuclei and well-evident cell contour; in contrast, (**B**) in a representative 40 μm-thick slice, neurons appear as densely basophilic spots, where neither nuclei nor nucleoli are visible, and cell contour is not defined.

Bar = 120 μm (**A**, **B**).

Figure 6. Different sampling procedures in the spinal cord and brainstem.

Different sampling procedures are required within the spinal cord compared with brainstem, in order to avoid counting twice the same motor neuron. Considering that sections are 7-8 μm thick and within spinal cord motor neurons possess a diameter up to 80 μm (**A**), one out of 10 sections are collected. (**B**) Within the brainstem, where the largest motor neurons possess a diameter up to 50 μm, one out of 7 sections are collected.

Figure 7. Measuring motor neuron size by using a stereology-like procedure.

Hypoglossal nucleus of the mouse brainstem, (**A**) as it appears in the Atlas table (Paxinos and Franklin, 2004; 7.32 mm posterior to bregma, red arrows), and (**B**) in a representative H&E-stained section, carried out at a corresponding level (dotted black line). The squared area is shown at high magnification in (**C**), where the maximum (42 μm) and minimum (28 μm) cell body diameter are

representatively drawn within a hypoglossal motor neuron. In this case the motor neuron diameter is considered to be 35 μm since it corresponds to the mean value between the maximum and minimum diameter.

Bars = 260 μm (**B**); 52 μm (**C**).

Figure 8. Identifying motor neuron site within the brainstem and spinal cord by using a stereology-like procedure.

Atlas tables of the mouse CNS are used to identify motor nuclei (**A**) ambiguous (Paxinos and Franklin, 2004; 6.86 mm posterior to the bregma) and (**B**) facial (Paxinos and Franklin, 2004; 6.24 mm posterior to the bregma) motor nuclei in the brainstem, and (**C**) within the lumbar spinal cord (Watson et al., 2009; about L6 level, red arrows). Representative sections of brainstem (**D** and **E**, stained with cresyl violet) and lumbar spinal cord (**F**, stained with H&E) are shown at the corresponding levels. In particular, dotted lines border ambiguous (**D**) and facial nuclei (**E**), as well as medial, intermediate and lateral columns of lumbar motor neurons (**F**). Ambiguous, facial and spinal cord motor neurons indicated by black arrows are shown at high magnification in the last line (**G-I**). Note the wider size of spinal cord motor neurons (**I**) compared with the brainstem ambiguous and facial motor neurons (**G** and **H**, respectively).

Bars = 400 μm (**D-F**); 15 μm (**G-I**).

Figure 9. Milestones in stereology-like procedure

The drawing summarizes the main steps of the stereology-like motor neuron count. These consist of: (**A**) dissection and embedding in paraffin of a specific tract of the spinal cord at the level of the lumbar enlargement; (**B**) count of H&E-stained motor neurons within non-consecutive 7-8 μm-thick slices at light microscopy, according to their placement in the ventral horn, size exclusion (threshold at 30 μm), shape and histochemical criteria (multipolar cell body with an intensely basophilic

nucleolus, large and pale nucleus and well-evident Nissl substance within the cytosol). (**C**) Data related to the number and size of motor neurons counted within each section are recorded on an excel file.

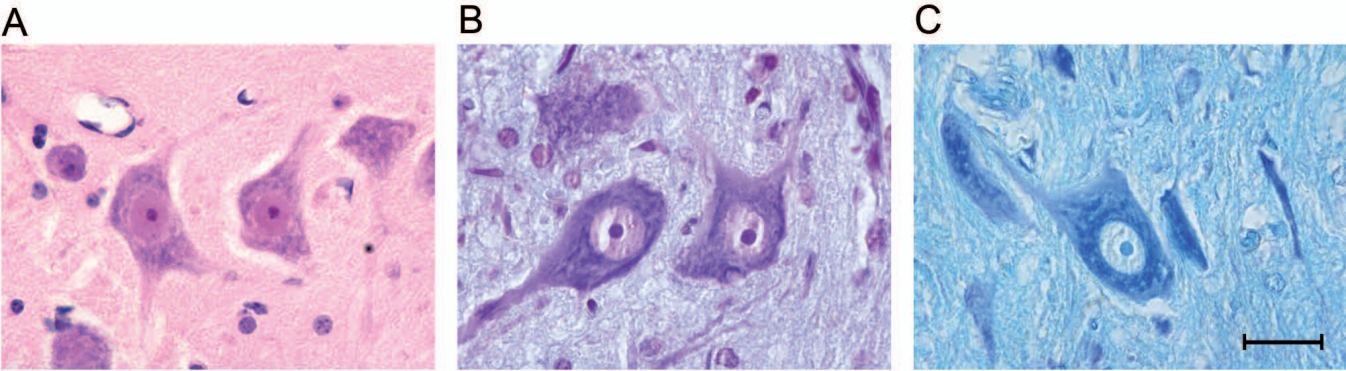
A
B
C

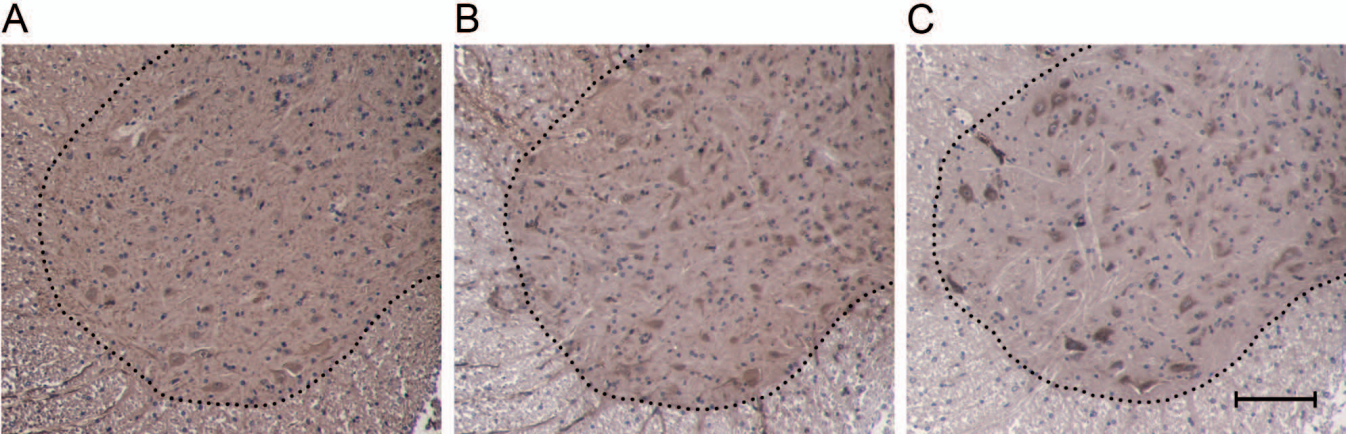
A
B
C

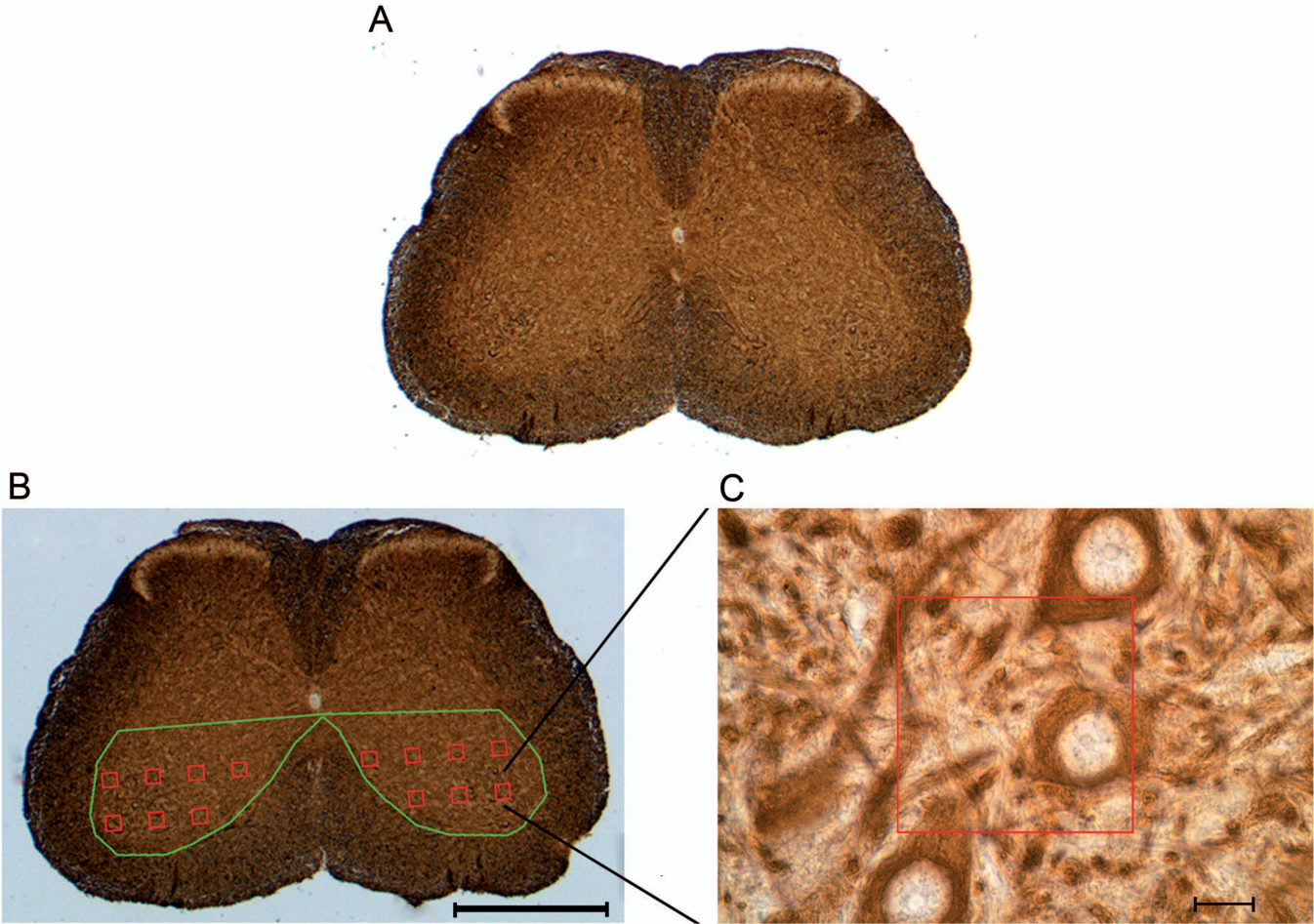
A
B
C

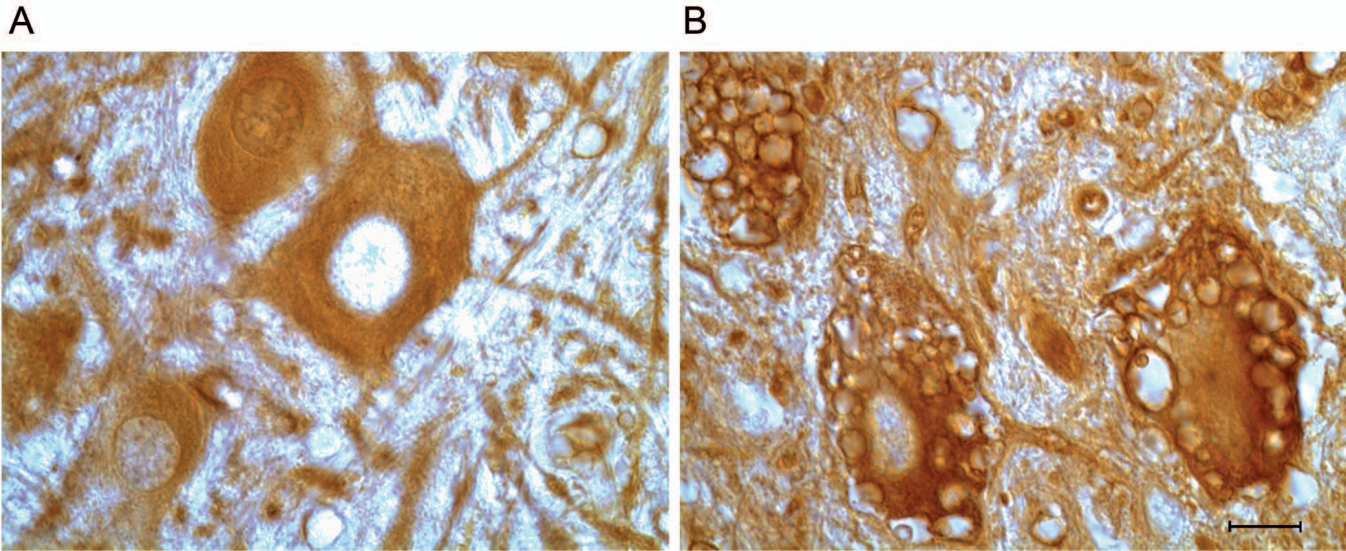
A
B

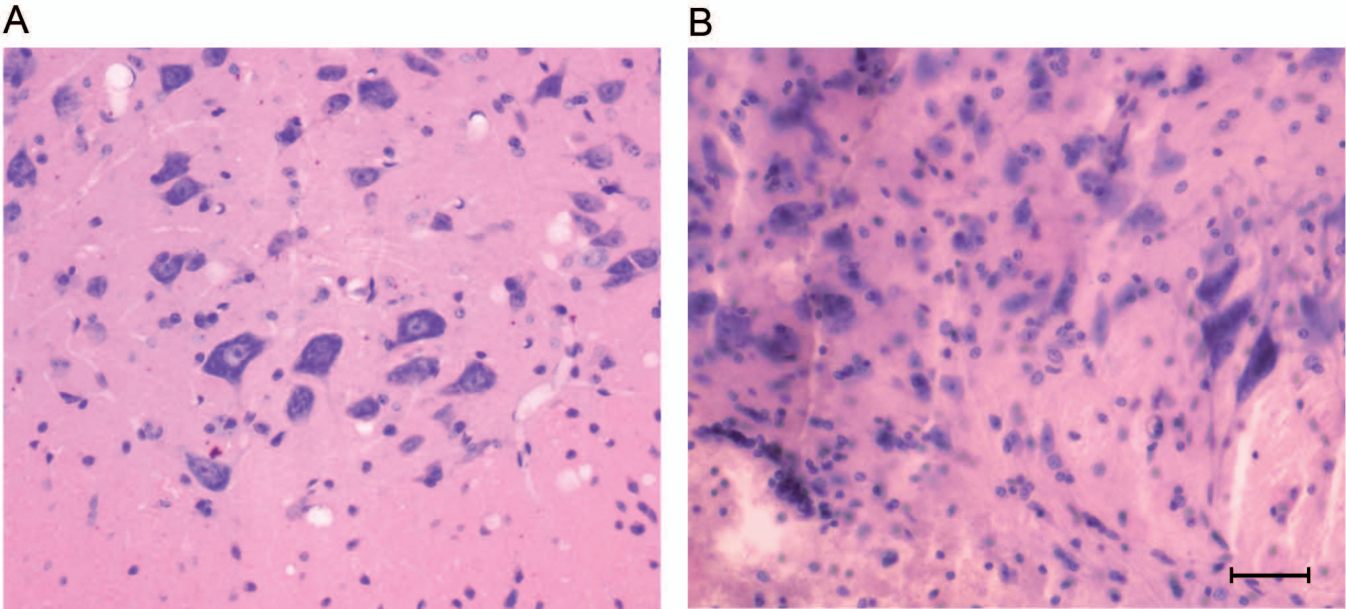
A
B

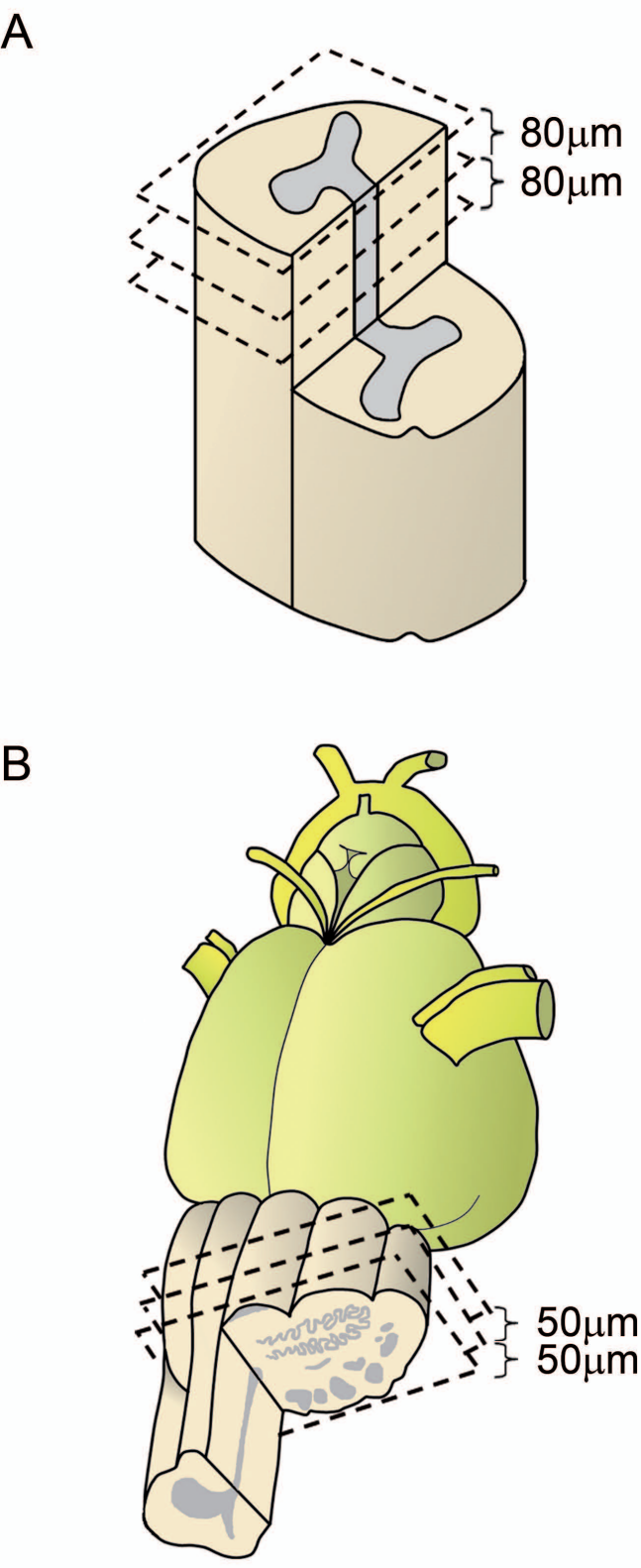
A
80μm
80μm
B
50μm
50μm

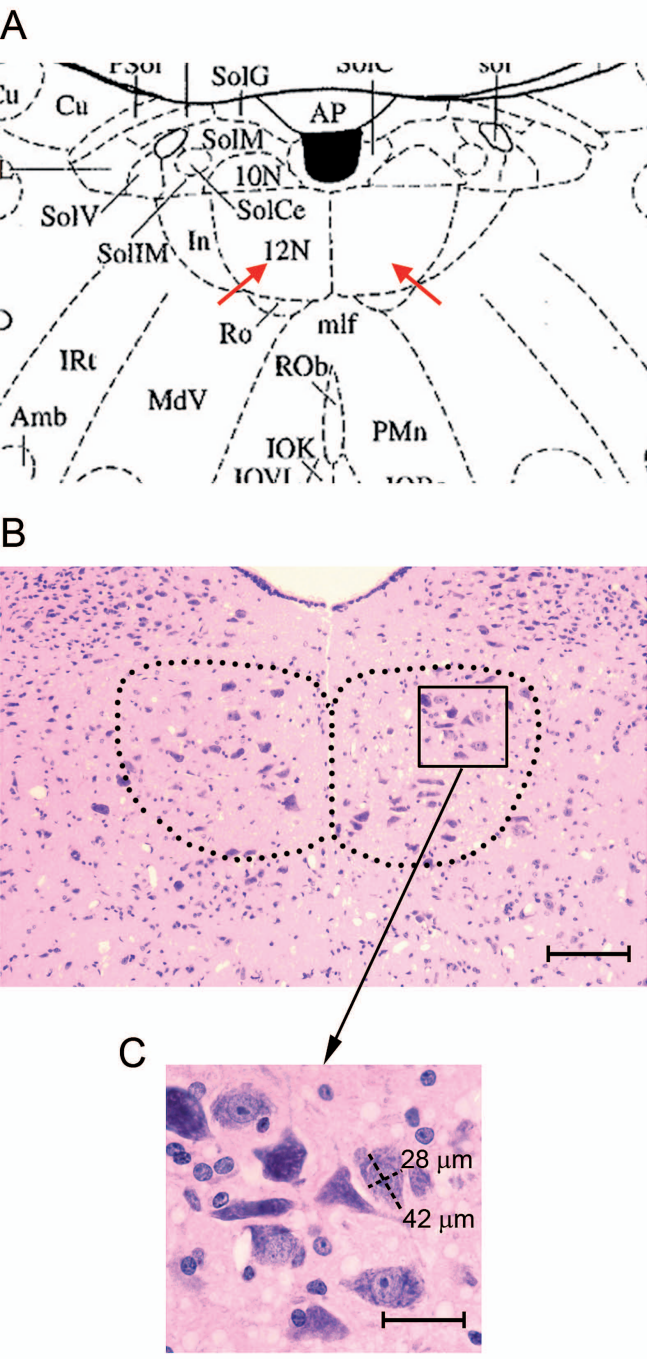
A
Cu
SolG
AP
SolM
10N
SolV
SolCe
SolIM
In
12N
Ro
mlf
IRt
ROb
MdV
Amb
PMn
IOK
B
C
28 µm
42 µm

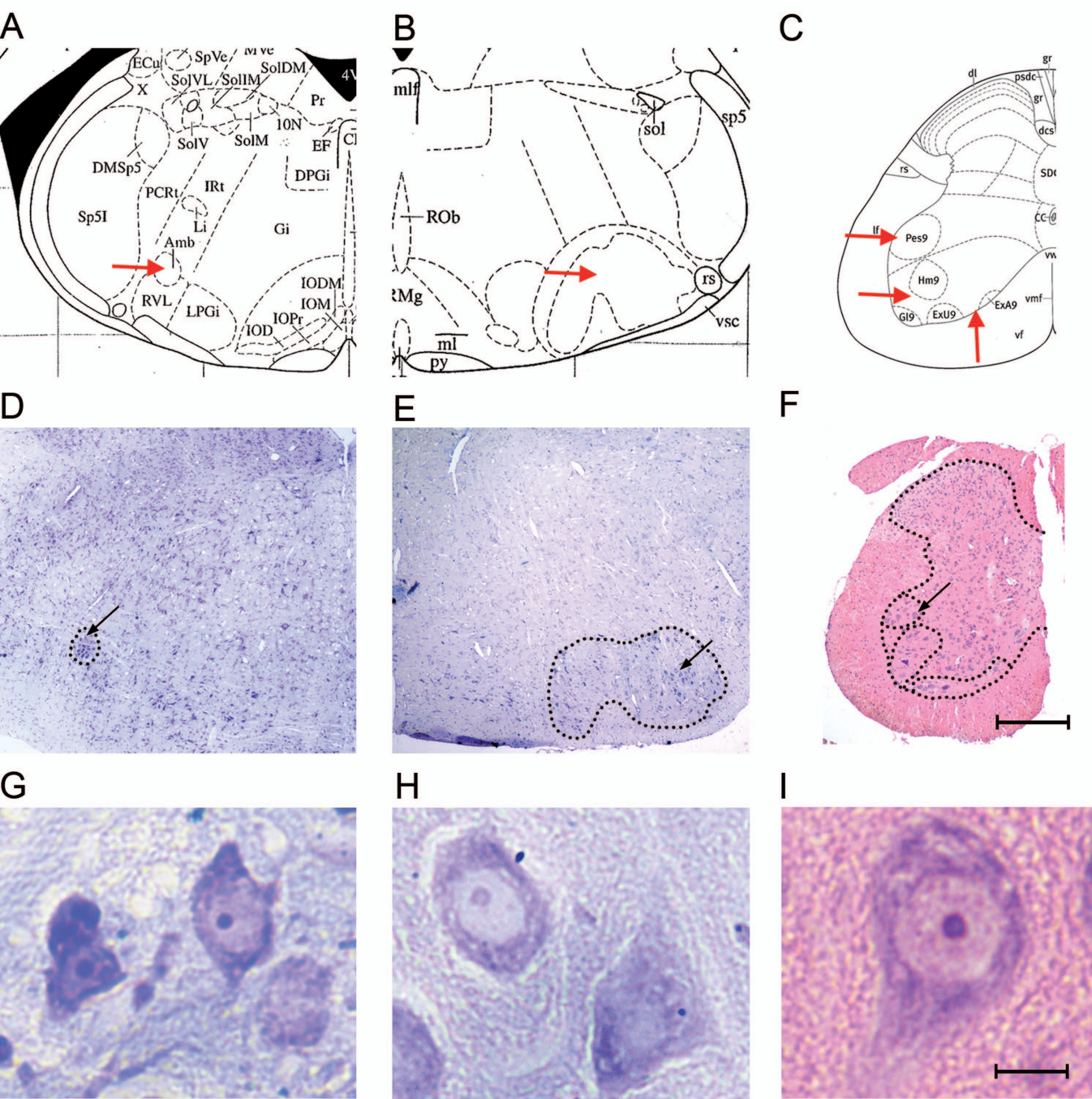
A
ECu
SpVe
SolDM
X
SolVL
SolIM
Pr
10N
SolV
SolM
EF
DMSp5
DPGi
PCRt
IRt
Sp5I
Li
Gi
Amb
IODM
RVL
LPGi
IOM
IOPr
IOD
B
mlf
sol
sp5
ROb
rs
Mg
vsc
ml
py
C
dl
gr
psdc
dcs
rs
lf
Pes9
Hm9
vmf
Gl9
ExU9
ExA9
vf
D
E
F
G
H
I

A

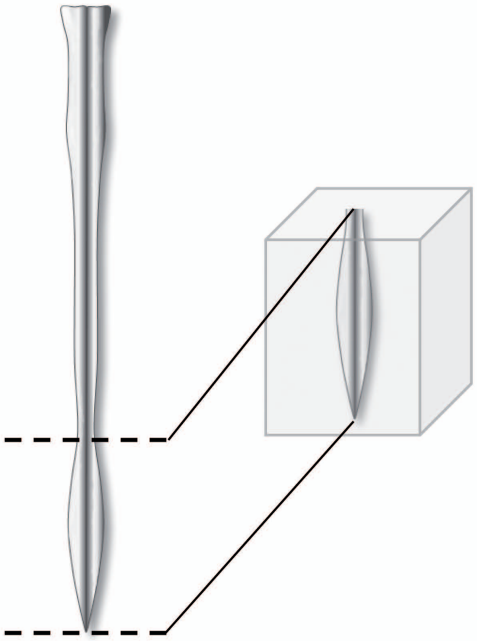

B

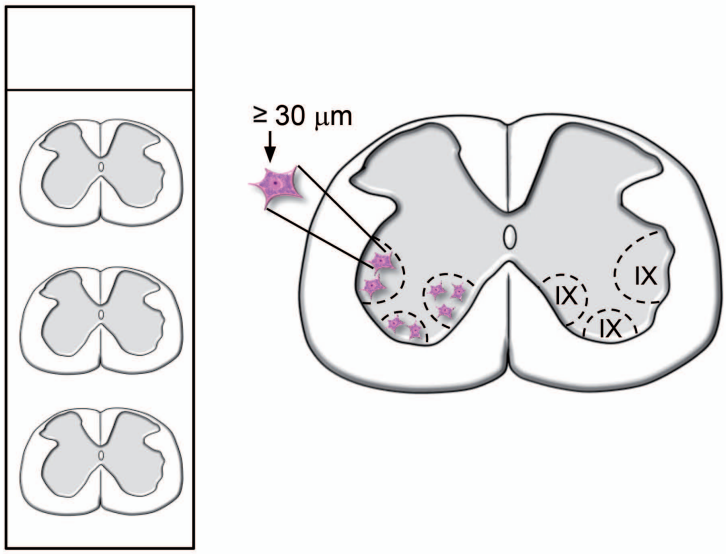

C

File Home Inserisci Layout di pagina Formule Dati Revisione Visualizza PDF Architect 4 Creator

Incolla Appunti | Times New Roman 12 Carattere | Allineamento | Generale Numeri | Formattazione condizionale Formatta come tabella Stili cella Stili

B34

	A	B	C	D	E	F	G	H	I	J	K	L	M	N	O
1	GROUP	WT													
2	ANIMAL	1													
4	SLICE	1		2		3		4		5		6		7	
5		sn	dx	sn	dx	sn	dx	sn	dx	sn	dx	sn	dx	sn	dx
6	# MN	12	11	13	13	11	12	10	12	11	10	11	12	10	13
7	Total MN #	3925													
8	MN diameter														
9		28.5	26.2	27.8	25.1	32.2	30.5	25.1	29.9	25.9	28.1	25.4	25.9	28.9	26.2
10		25.3	25.6	30.0	30.0	25.1	26.7	25.4	35.7	32.9	26.7	26.2	28.9	34.0	25.9
11		26.7	30.8	25.9	31.6	27.0	27.1	30.0	30.3	27.0	27.1	25.7	28.3	25.4	27.5
12		27.3	25.3	28.0	27.5	26.6	27.5	32.0	29.3	26.3	25.8	31.3	29.2	28.4	28.3
13		25.2	29.1	29.3	26.5	26.9	27.7	28.8	25.6	30.1	30.3	28.5	25.2	25.9	26.3
14		26.0	25.9	25.4	26.6	27.5	29.7	29.3	25.9	26.2	28.1	30.5	28.1	27.5	25.8
15		30.7	26.3	26.6	25.6	29.8	31.0	26.0	27.4	25.1	25.4	27.6	30.6	26.1	27.4
16		25.2	28.4	28.8	26.8	28.2	29.3	27.1	26.6	25.9	31.1	28.3	26.5	26.4	25.4
17		27.0	32.7	29.2	26.2	30.5	25.7	27.0	25.4	25.4	29.5	26.6	26.1	30.8	26.1
18		25.9	26.4	31.9	29.5	28.0	27.1	26.4	31.2	31.9	30.0	27.3	25.9	29.6	26.9
19		32.3	29.8	29.7	27.1	28.4	25.4		26.6	28.5		29.1	26.1		31.5
20		28.5		28.4	32.0		26.8		27.3				25.4		26.1
21				25.3	28.6										28.0
22															
23															
24															
25	Average MN diameter	27.7													